© 2020 Wiley-VCH GmbH

ADVANCED MATERIALS

Supporting Information

for *Adv. Mater.*, DOI: 10.1002/adma.202003730

Blocking Ion Migration Stabilizes the High Thermoelectric Performance in Cu_2Se Composites

Dongwang Yang, Xianli Su, Jun Li, Hui Bai, Shanyu Wang, Zhi Li, Hao Tang, Kechen Tang, Tingting Luo, Yonggao Yan, Jinsong Wu, Jihui Yang, Qingjie Zhang, Ctirad Uher, Mercouri G. Kanatzidis,* and Xinfeng Tang**

Blocking Ion Migration Stabilizes the High Thermoelectric Performance in Cu_2Se Composites

Dongwang Yang[a†], Xianli Su[a,e†], Jun Li[a], Hui Bai[a,b], Shanyu Wang[c], Zhi Li[a,e], Hao Tang[a], Kechen Tang[a], Tingting Luo[a,b], Yonggao Yan[a], Jinsong Wu[a,b], Jihui Yang[c], Qingjie Zhang[a], Ctirad Uher[d], Mercouri. G. Kanatzidis[e] and Xinfeng Tang[a*]

[a]*State Key Laboratory of Advanced Technology for Materials Synthesis and Processing, Wuhan University of Technology, Wuhan 430070, China.*

[b]*Nanostructure Research Centre, Wuhan University of Technology, Wuhan 430070, China.*

[c]*Materials Science and Engineering Department, University of Washington, Seattle, Washington 98195, USA.*

[d]*Department of Physics, University of Michigan, Ann Arbor, Michigan 48109, USA.*

[e]*Department of Chemistry, Northwestern University, Evanston, Illinois 60208, USA*.

†These authors contributed equally to this work.

Correspondence and requests for materials should be addressed to Jihui Yang (jihuiy@uw.edu), Mercouri G. Kanatzidis (m-kanatzidis@northwestern.edu), Xinfeng Tang (tangxf@whut.edu.cn)

Synthesis of Cu_2Se_{1+x} / yBiCuSeO composites: Cu (4N, 200 mesh), Se (5N, 200 mesh), and Bi_2SeO_2 (synthesized by thermal explosion method, 200 mesh) [1] powders were weighed according to Equation 1 (x=0, 0.005, 0.010, 0.015, 0.020; y=0, 0.05, 0.1, 0.3, 0.5 mol%),

$$(2+y)\ Cu + (1+x+y/2)\ Se + y/2\ Bi_2SeO_2 = Cu_2Se_{1+x} / yBiCuSeO \quad (1)$$

Thoroughly mixed and hand ground powders were cold pressed into pellets at a pressure of 10 MPa for 5 min. The pellets were ignited by Joule heating a carbon foil in vacuum in a homemade SHS apparatus [1]. The as-reacted product was hand ground and consolidated by plasma activated sintering (PAS) (PAS-III-Ed, Elenix, Japan) under 40 MPa in vacuum at 973 K for 3 min.

At room temperature, when the Se content is in the range of 33.3-33.8% (35.3-36.4%), the $Cu_2Se_{1+\delta}$ compound adopts a stable α (β) phase [2]. Therefore, in the present study of Cu_2Se_{1+x} / yBiCuSeO, the range of x (aka the Se excess) is designed to be 0 ~ 0.02.

Structural characterization and thermoelectric properties: Phase purity of all samples was inspected by X-ray powder diffraction (Empyrean, Cu K_α line, PANalytical, Holland). Images of freshly fractured surfaces were taken by field emission scanning electron microscopy (FESEM) (SU8000, Hitachi, Japan) with energy-dispersive X-ray spectroscopy (EDS) (XFlash6160, BRUKER, Germany). A direct characterization of the samples' atomic structures was carried out on transmission electron microscopy (Talos F200s, FEI) and double CS-corrected transmission electron microscopy (Titan Themis G2 60-300, FEI). The samples for TEM observation were prepared by focused ion beam (FIB) milling (Helios Nanolab G3 UC, FEI). The ultraviolet photoemission spectroscopy (UPS) measurements were performed on a Thermo Fisher ESCALAB 250 Xi instrument with an He I radiation source ($h\nu$ = 21.2 eV). Electrical transport measurements were conducted using an ULVAC-RIKO ZEM-3 (Ulvac, Japan) instrument under a helium atmosphere from 300 K to 973 K. The electrical conductivity (σ) and the Hall coefficient (R_H) between 10 K and 300 K were measured on a Physical Properties Measurement System (PPMS-9, Quantum Design, USA). The high temperature electrical conductivity (σ) and the Hall coefficient (R_H) between 300 K and 700 K were measured using the van der Pauw technique under a reversible magnetic field of 1.5 T. The effective carrier concentration (n_H) was calculated by the formula: $n_H=1/eR_H$, where e is the electron charge. The Hall mobility

follows from $\mu_{\square}=\sigma R_H$. The thermal conductivity was calculated using the relation $\kappa_{\square}=D\times C_p\times\rho$, where the thermal diffusivity D was measured using a LFA457 (Netzsch, Germany) laser flash apparatus, high temperature specific heat capacity C_p was measured using Q2000 (TA, USA), the bulk density ρ was measured by Archimedes method. The uncertainties were estimated to be 3% for thermal diffusivity, specific heat capacity, and electrical conductivity, and 5% for the Seebeck coefficient, which results in an uncertainty of 11% for ZT.

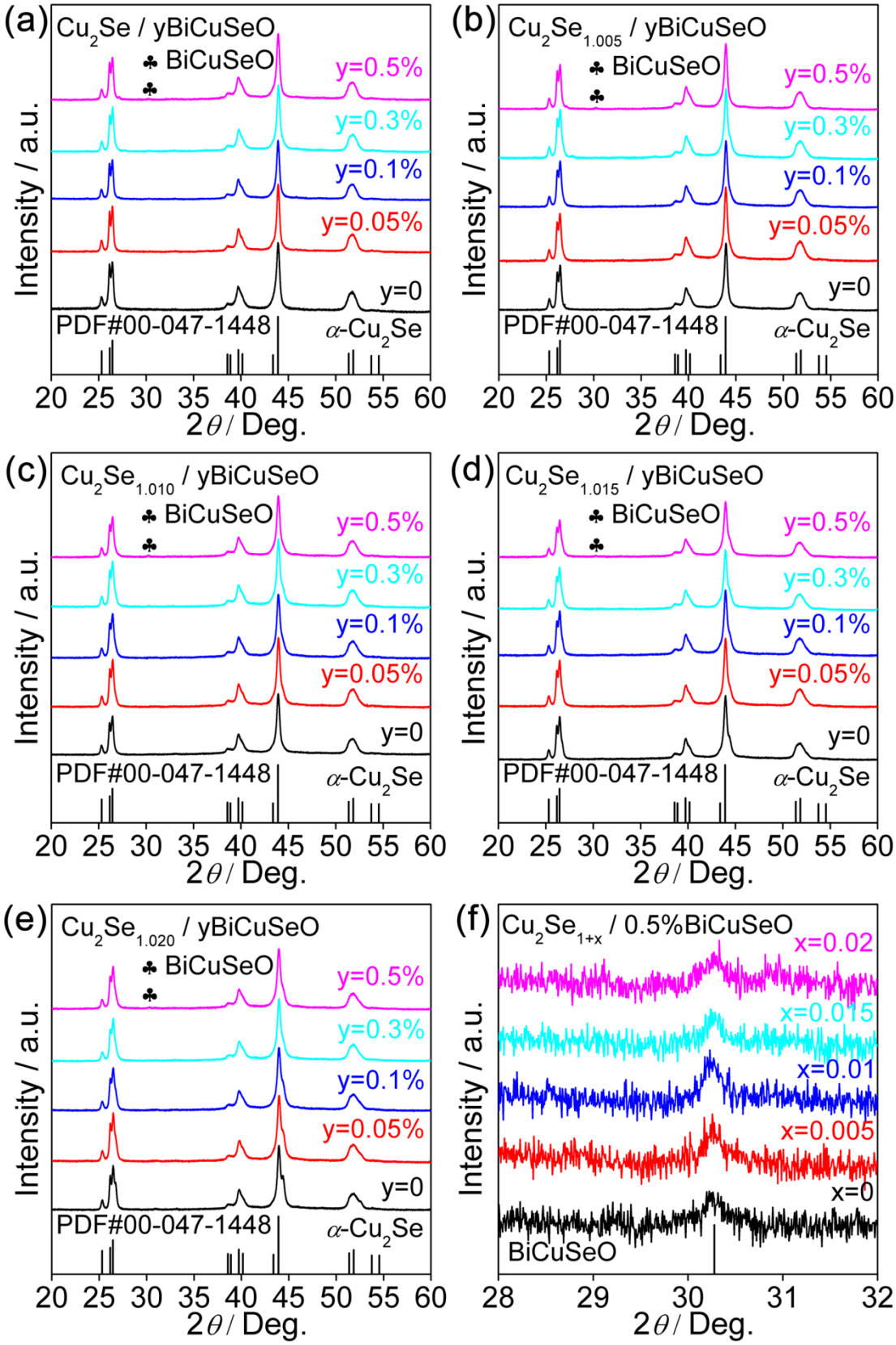

Figure S1. Phase compositions of Cu_2Se_{1+x} / yBiCuSeO (x=0, 0.005, 0.010, 0.015, 0.020; y=0, 0.05, 0.1, 0.3, 0.5 mol%) composites obtained by self-propagating high-temperature synthesis (SHS), followed by plasma activated sintering (PAS). The presence of BiCuSeO was detected at y > 0.5%.

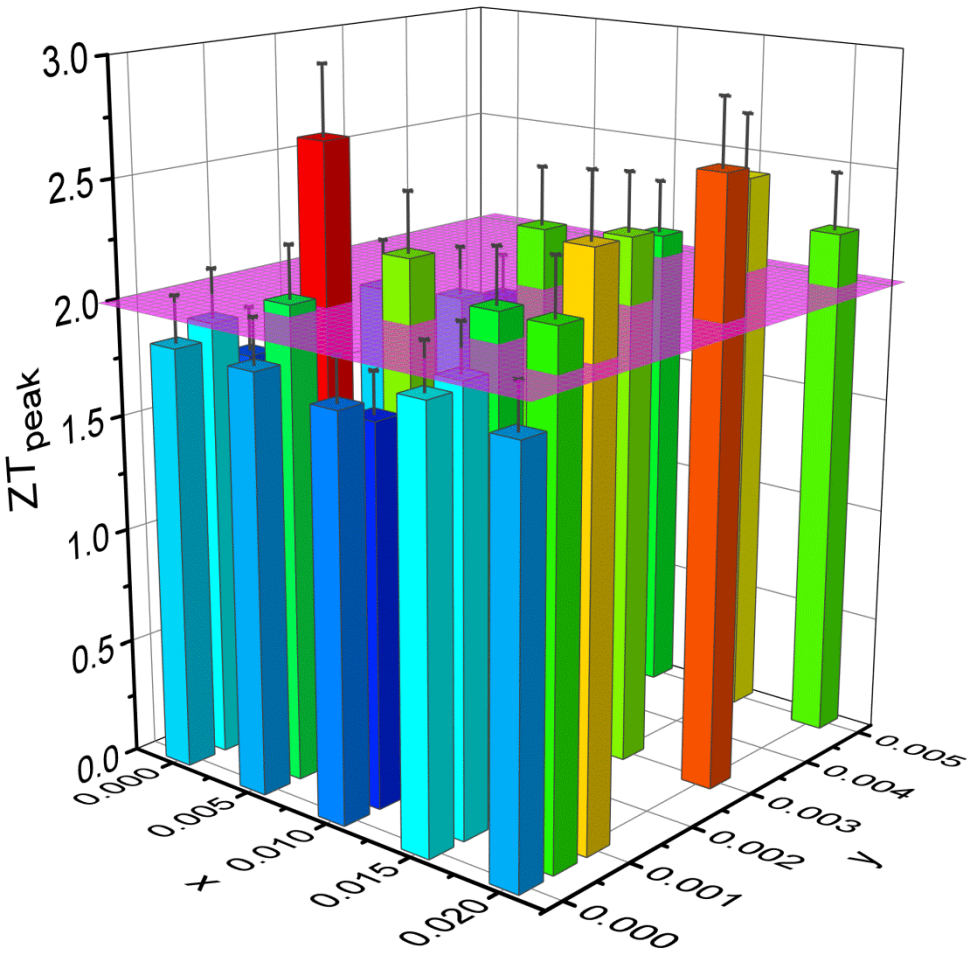

Figure S2. The ZT_{peak} of Cu_2Se_{1+x} / yBiCuSeO composites at 973K

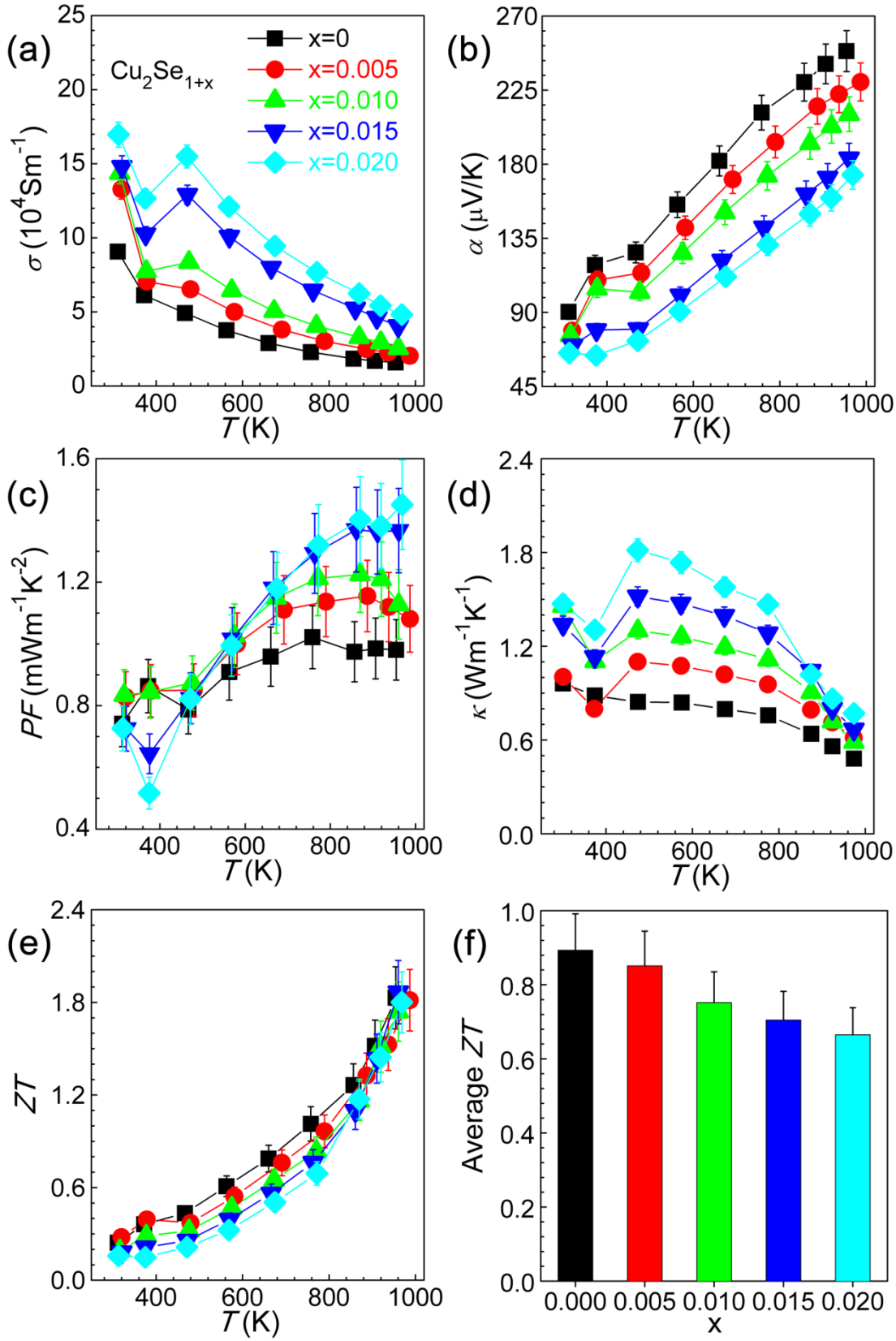

Figure S3. Thermoelectric properties of Cu_2Se_{1+x} without BiCuSeO. (a) electrical conductivity; (b) Seebeck coefficient; (c) power factor; (d) thermal conductivity; (e) *ZT*; (f) average *ZT* values between 400 K and 973 K.

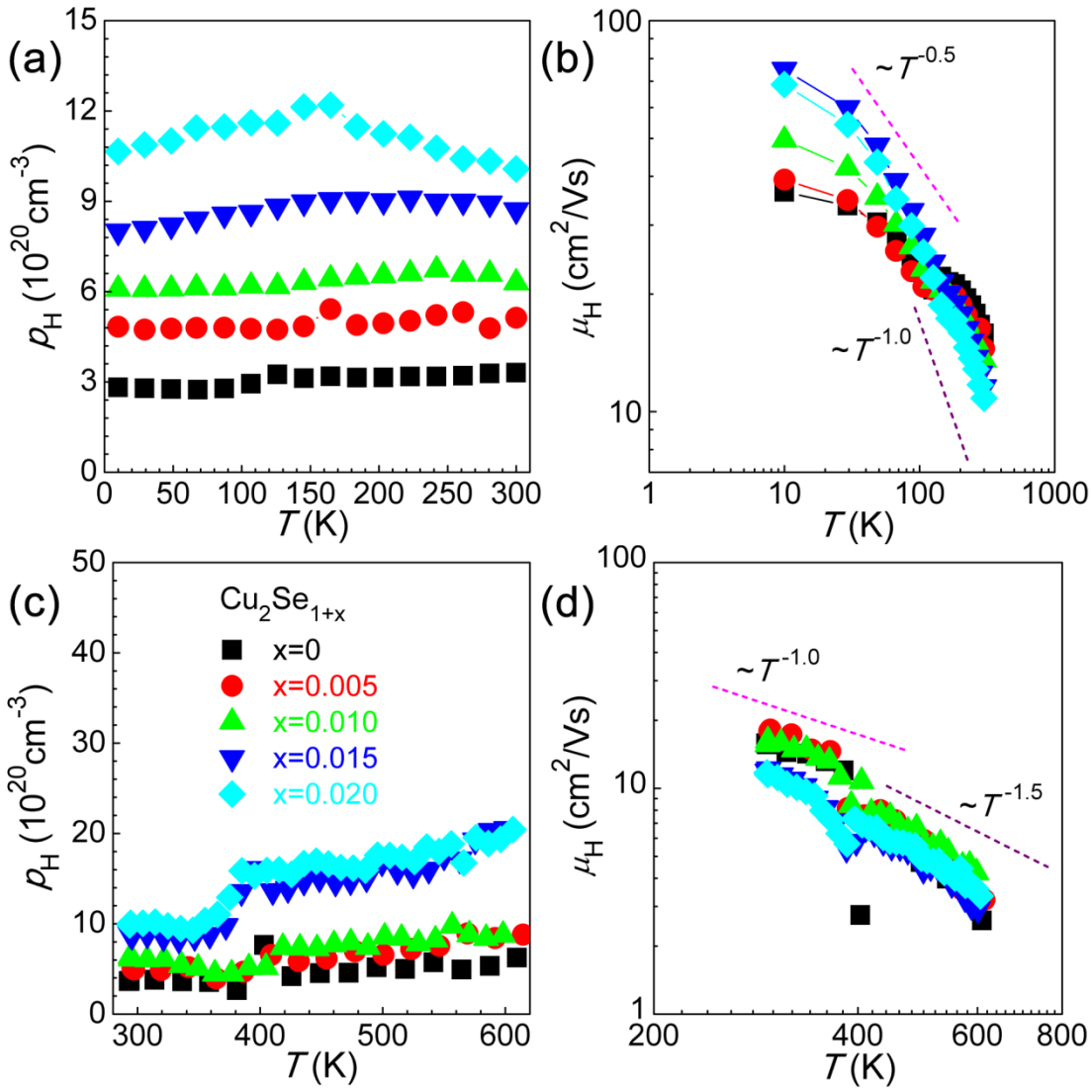

Figure S4. Electrical transport properties of Cu_2Se_{1+x}. (a) low temperature carrier concentration; (b) low temperature carrier mobility; (c) high temperature carrier concentration; (d) high temperature carrier mobility.

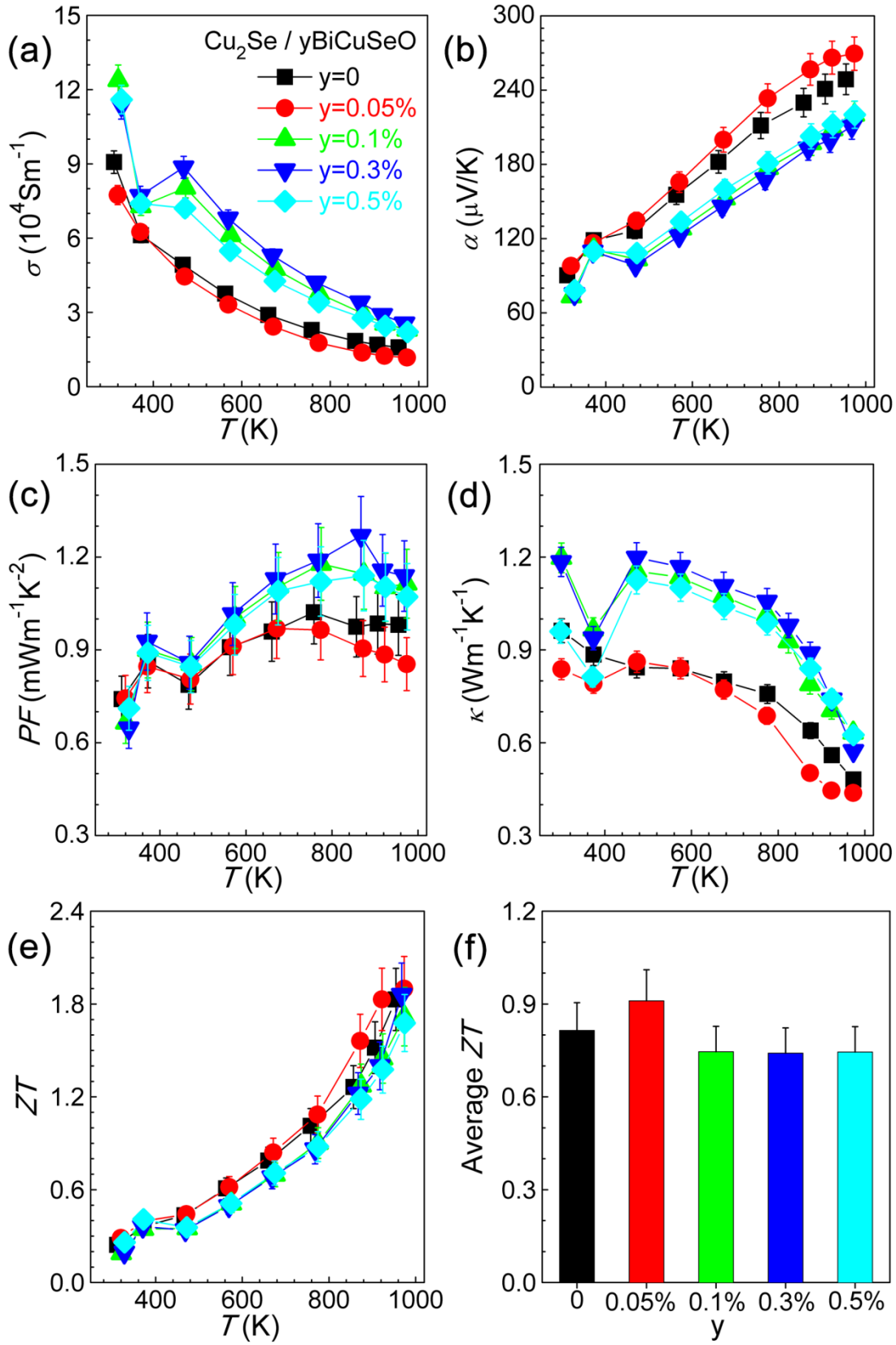

Figure S5. Thermoelectric properties of Cu_2Se / yBiCuSeO. (a) electrical conductivity; (b) Seebeck coefficient; (c) power factor; (d) thermal conductivity; (e) *ZT*; (f) average *ZT* values between 400 K and 973 K.

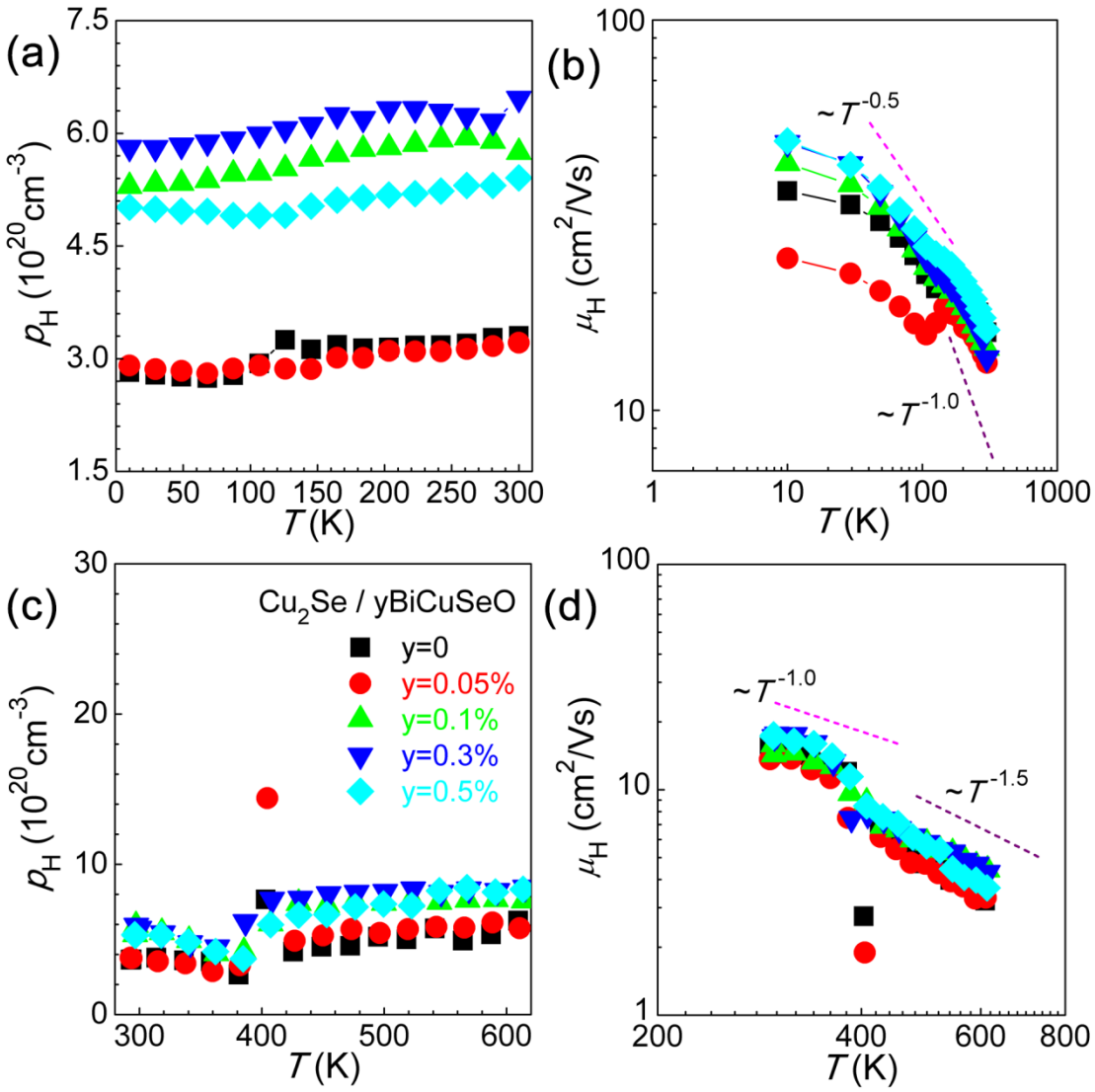

Figure S6. Electrical transport properties of Cu_2Se / yBiCuSeO. (a) low temperature carrier concentration; (b) low temperature carrier mobility; (c) high temperature carrier concentration; (d) high temperature carrier mobility.

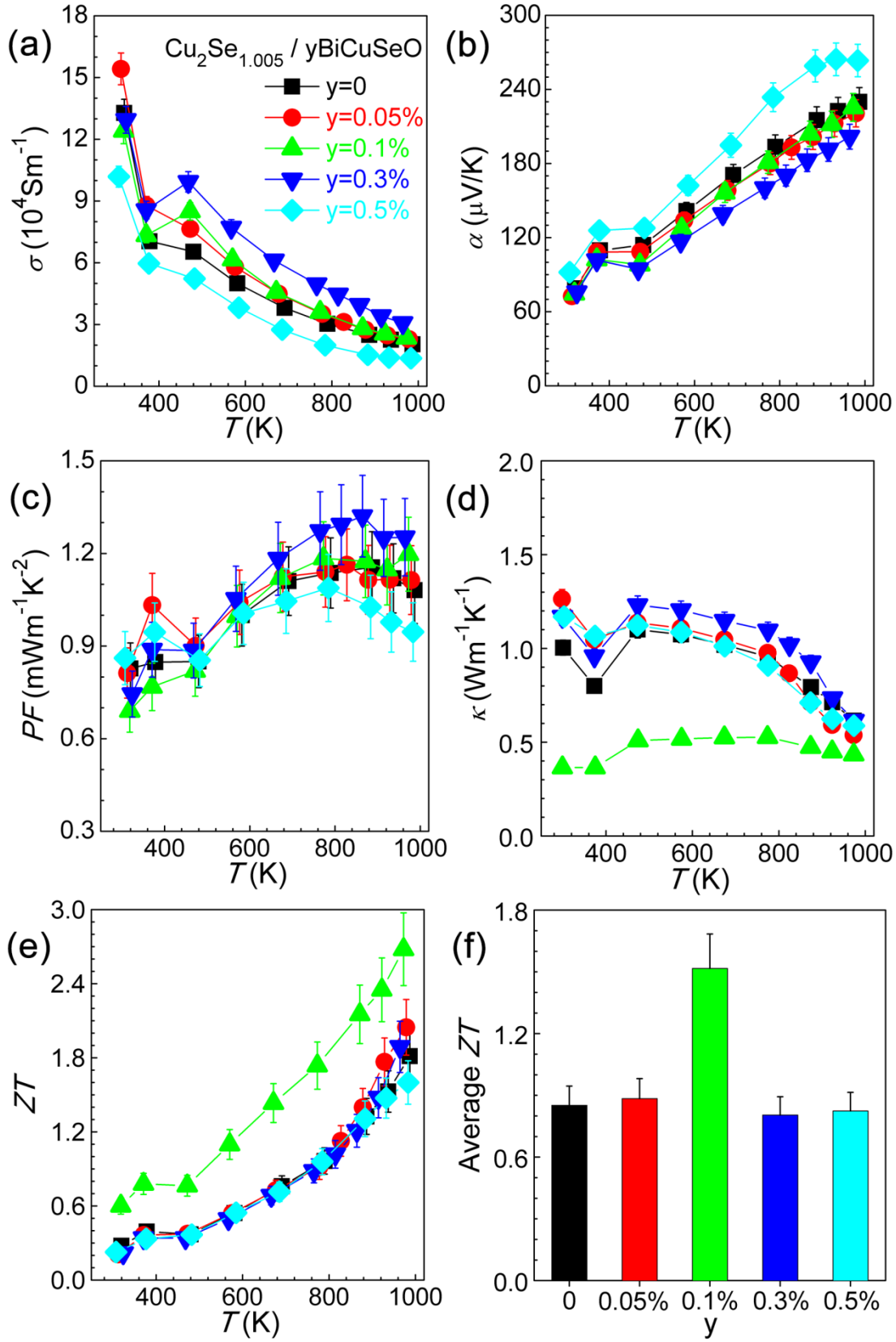

Figure S7. Thermoelectric properties of $Cu_2Se_{1.005}$ / yBiCuSeO. (a) electrical conductivity; (b) Seebeck coefficient; (c) power factor; (d) thermal conductivity; (e) *ZT*; (f) average *ZT* values between 400 K and 973 K.

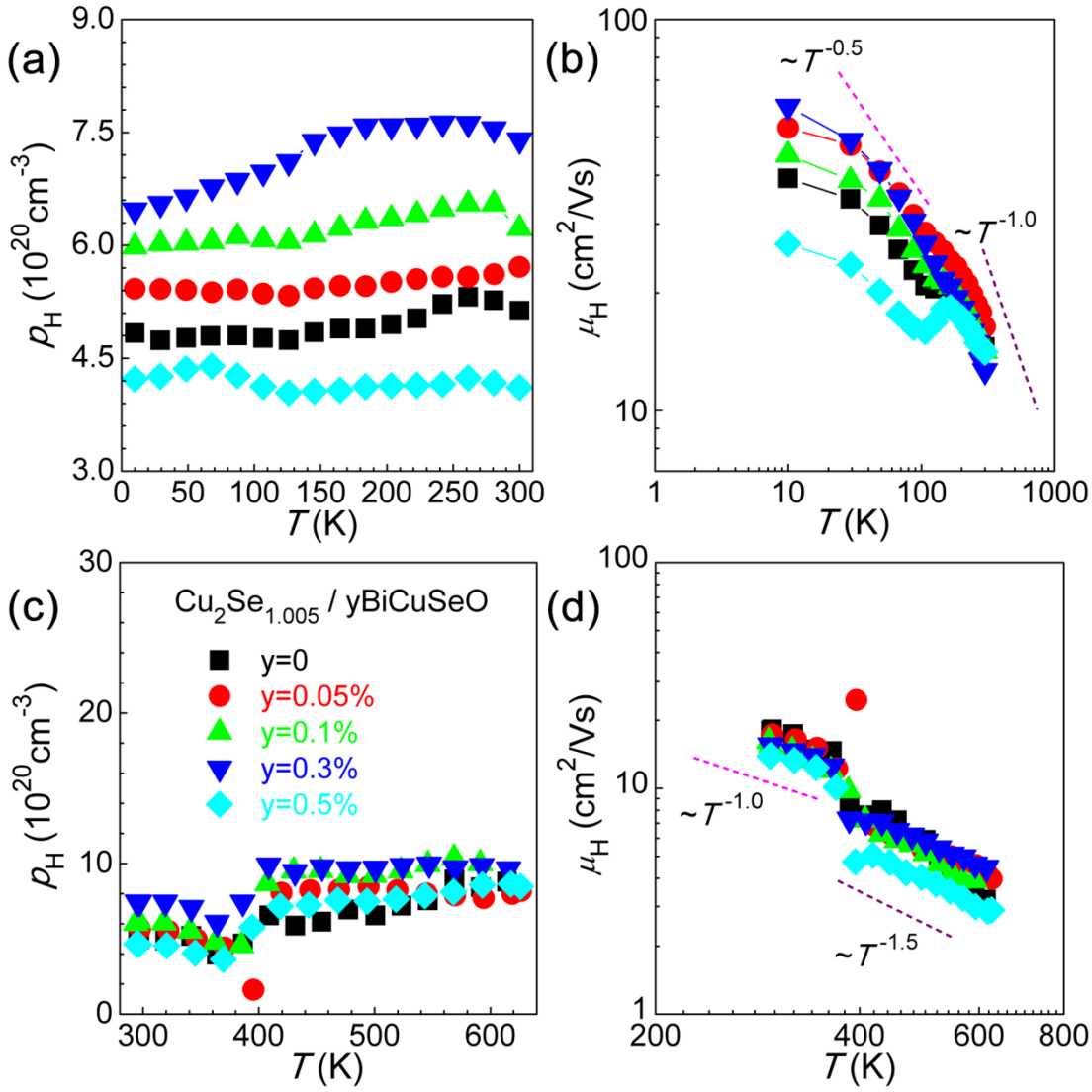

Figure S8. Electrical transport properties of $Cu_2Se_{1.005}$ / yBiCuSeO. (a) low temperature carrier concentration; (b) low temperature carrier mobility; (c) high temperature carrier concentration; (d) high temperature carrier mobility.

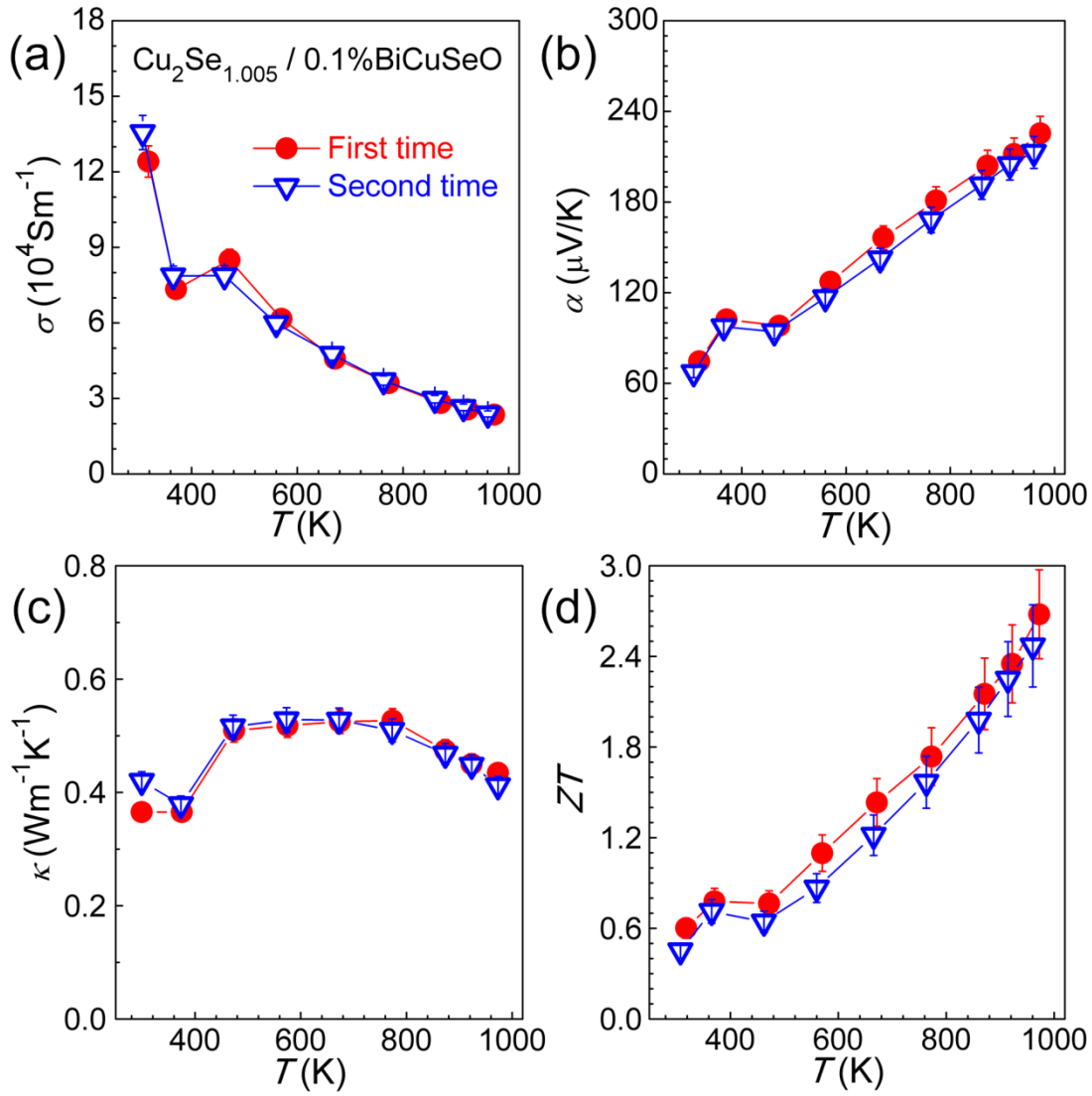

Figure S9. Thermoelectric properties of $Cu_2Se_{1.005}$ / 0.1 mol% BiCuSeO after two thermal cycles between room temperature and 973 K.

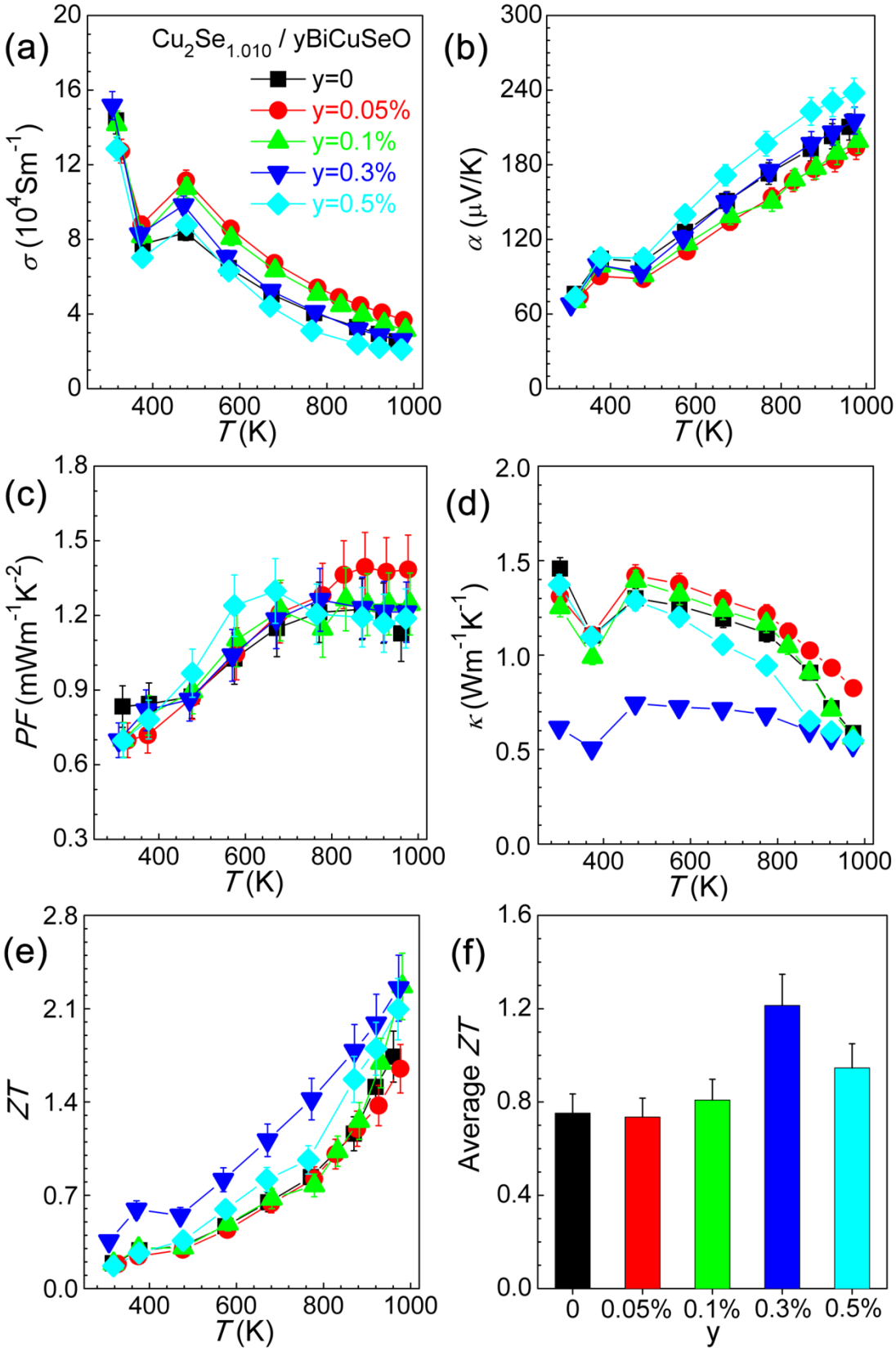

Figure S10. Thermoelectric properties of $Cu_2Se_{1.010}$ / yBiCuSeO. (a) electrical conductivity; (b) Seebeck coefficient; (c) power factor; (d) thermal conductivity; (e) *ZT*; (f) average *ZT* values between 400 K and 973 K.

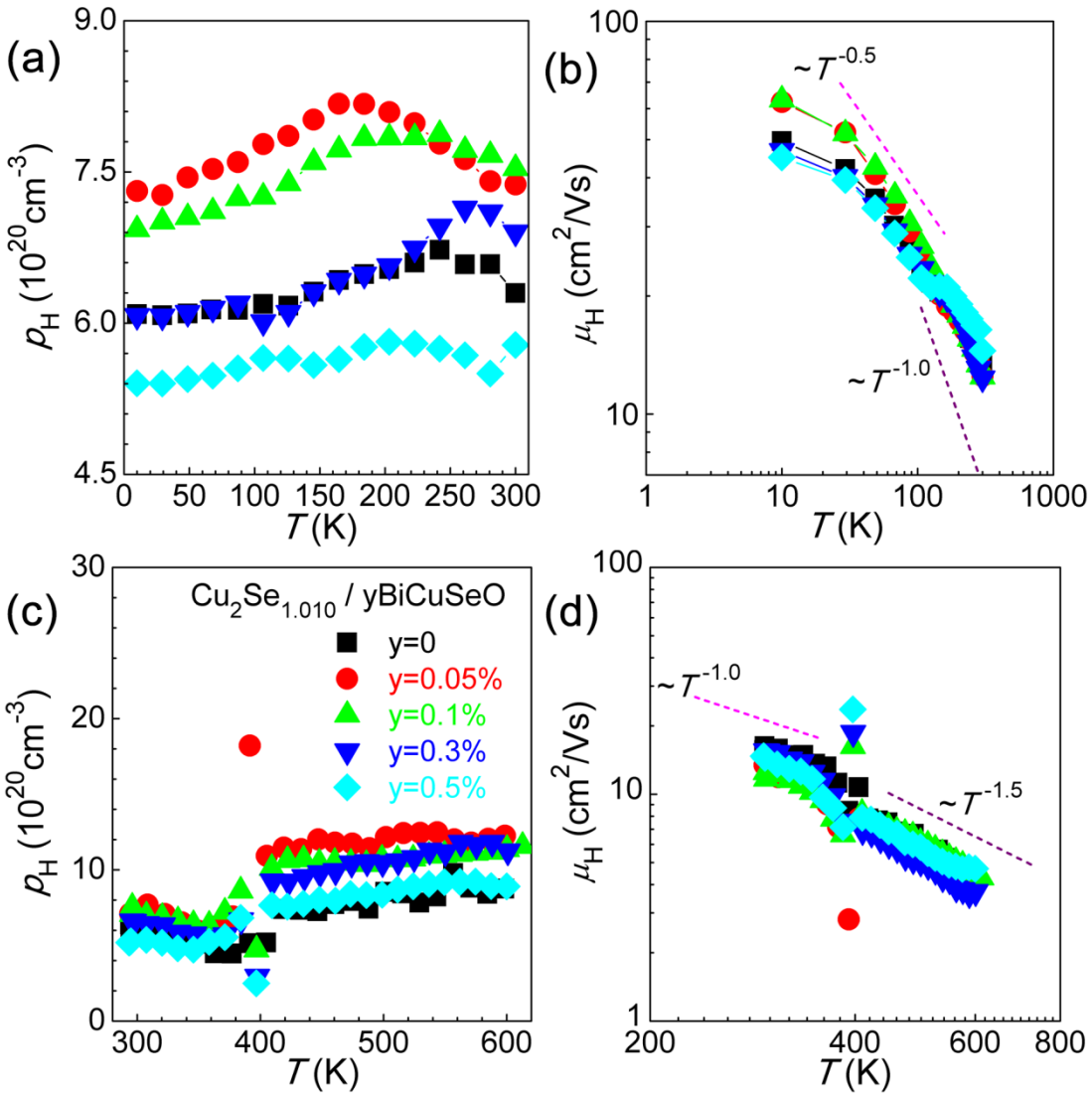

Figure S11. Electrical transport properties of $Cu_2Se_{1.010}$ / yBiCuSeO. (a) low temperature carrier concentration; (b) low temperature carrier mobility; (c) high temperature carrier concentration; (d) high temperature carrier mobility.

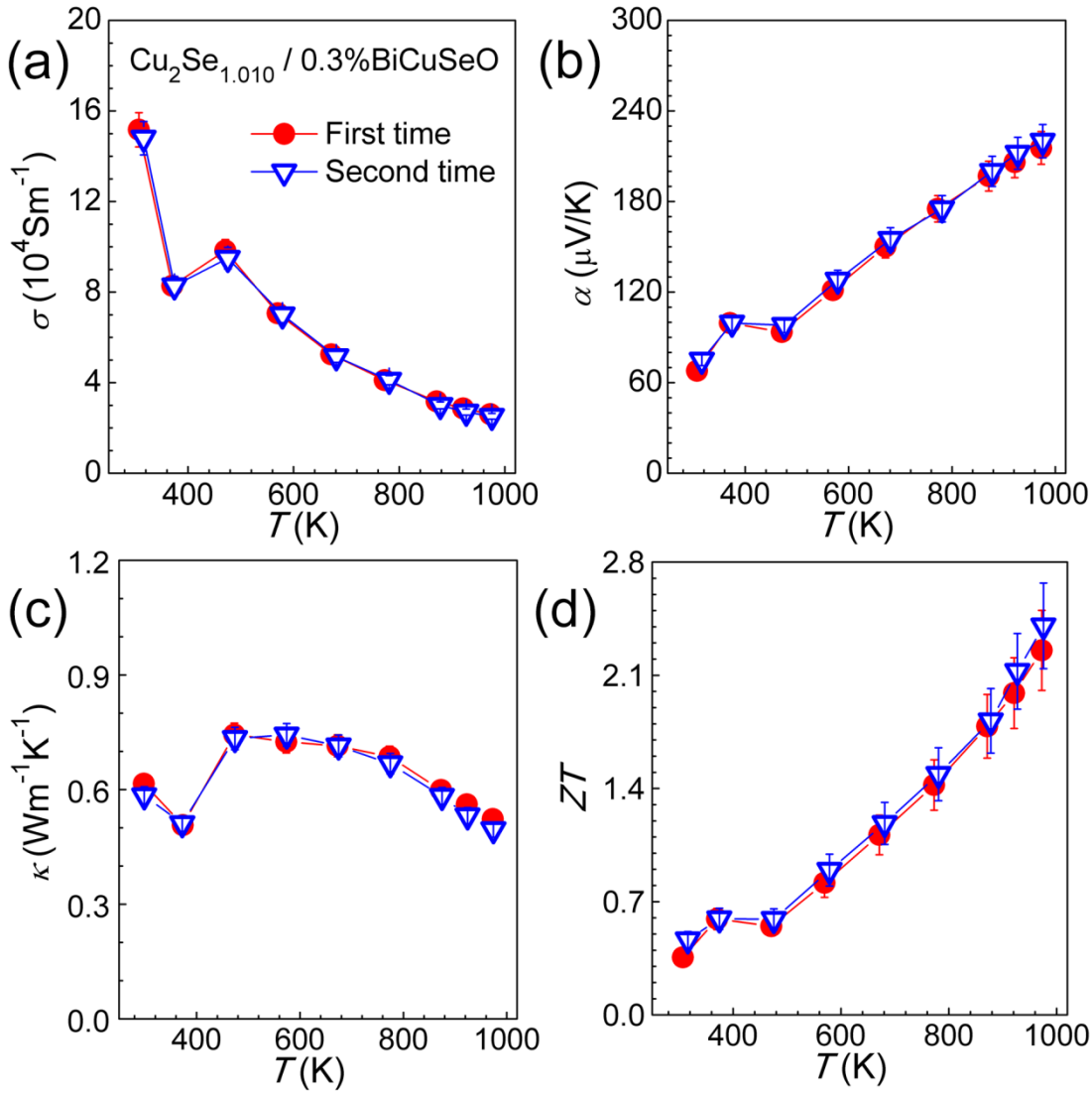

Figure S12. Thermoelectric properties of $Cu_2Se_{1.010}$ / 0.3 mol% BiCuSeO after two thermal cycles between room temperature and 973 K.

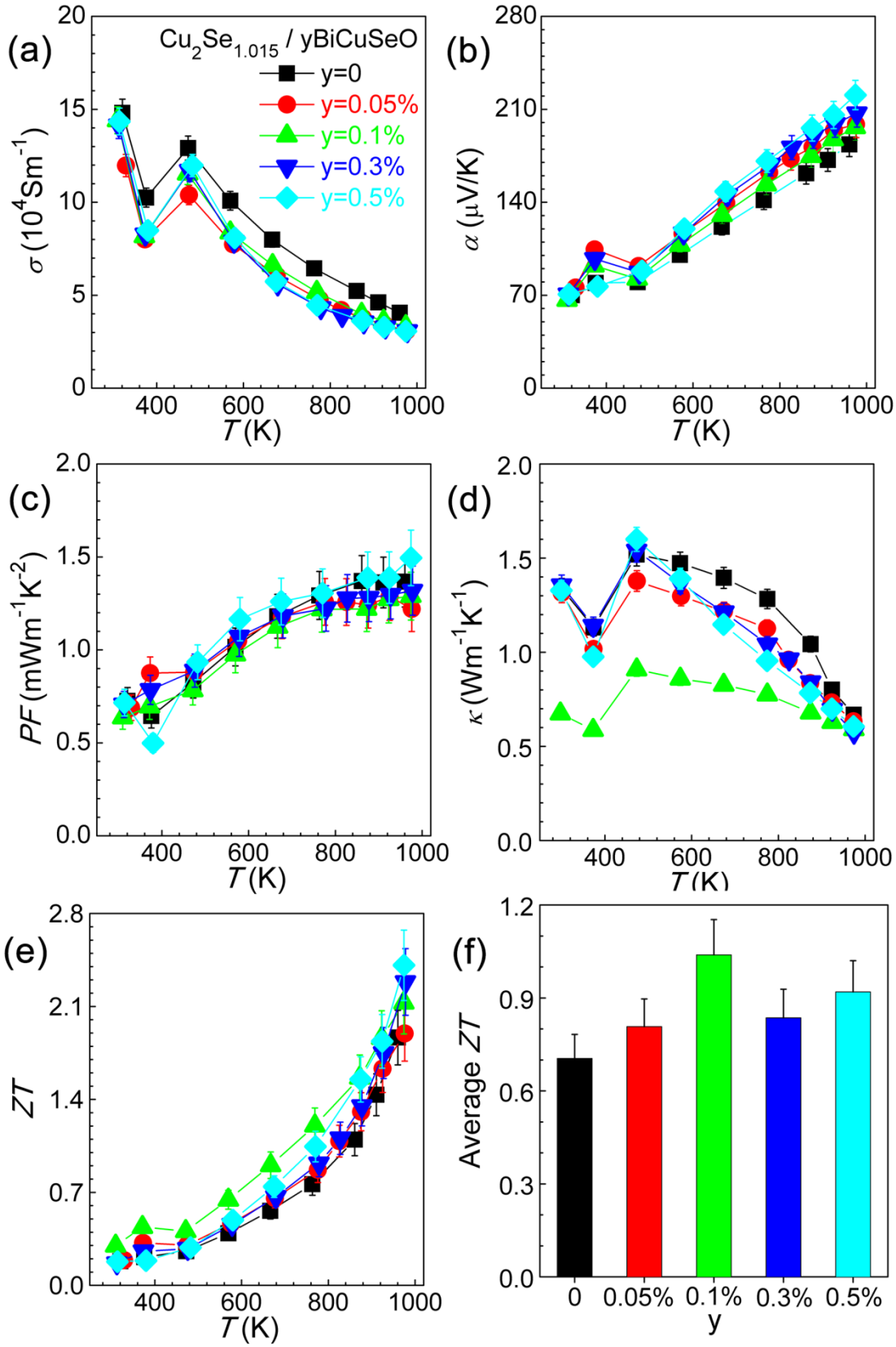

Figure S13. Thermoelectric properties of $Cu_2Se_{1.015}$ / yBiCuSeO. (a) electrical conductivity; (b) Seebeck coefficient; (c) power factor; (d) thermal conductivity; (e) *ZT*; (f) average *ZT* values between 400 K and 973 K.

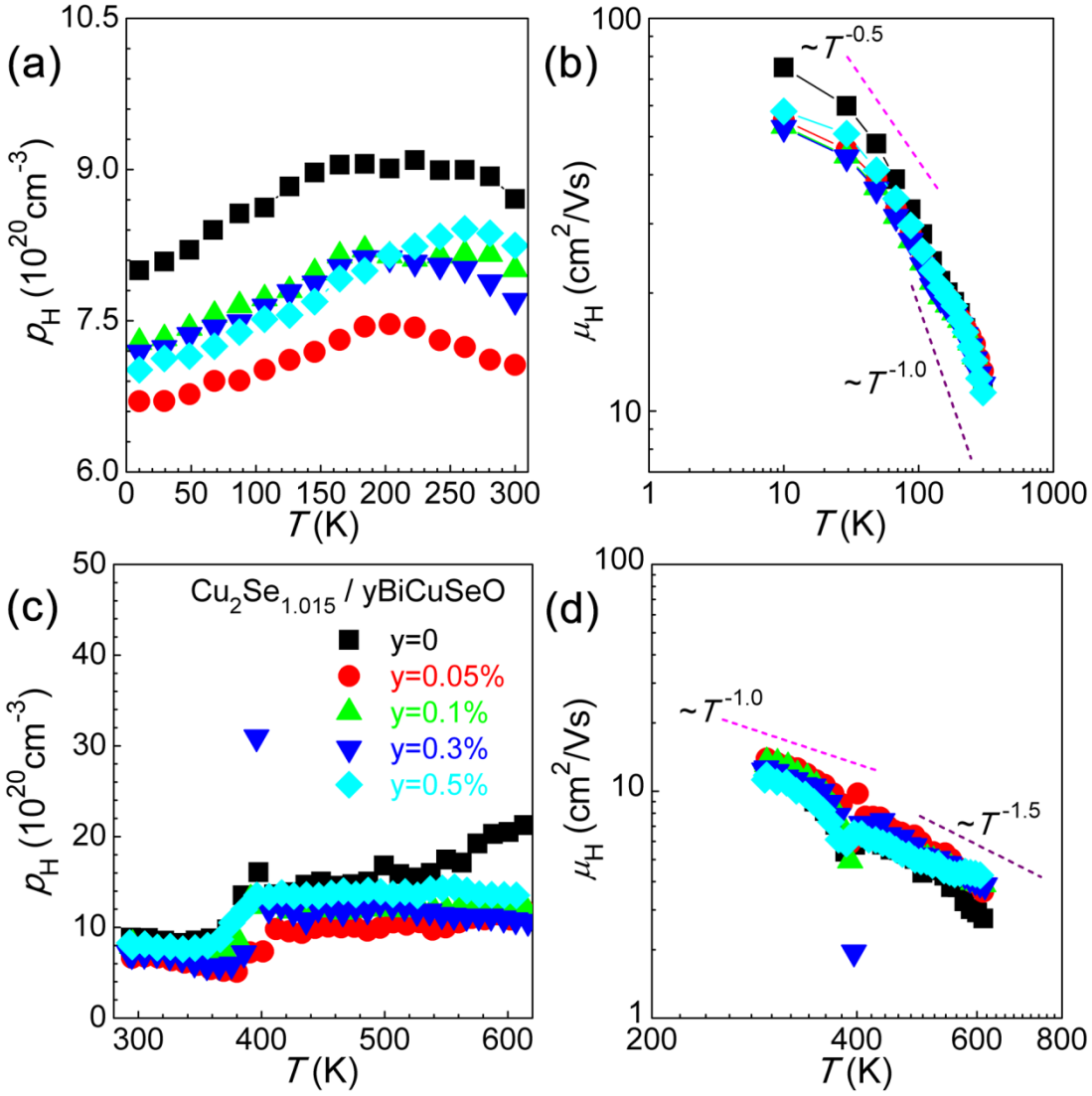

Figure S14. Electrical transport properties of $Cu_2Se_{1.015}$ / yBiCuSeO. (a) low temperature carrier concentration; (b) low temperature carrier mobility; (c) high temperature carrier concentration; (d) high temperature carrier mobility.

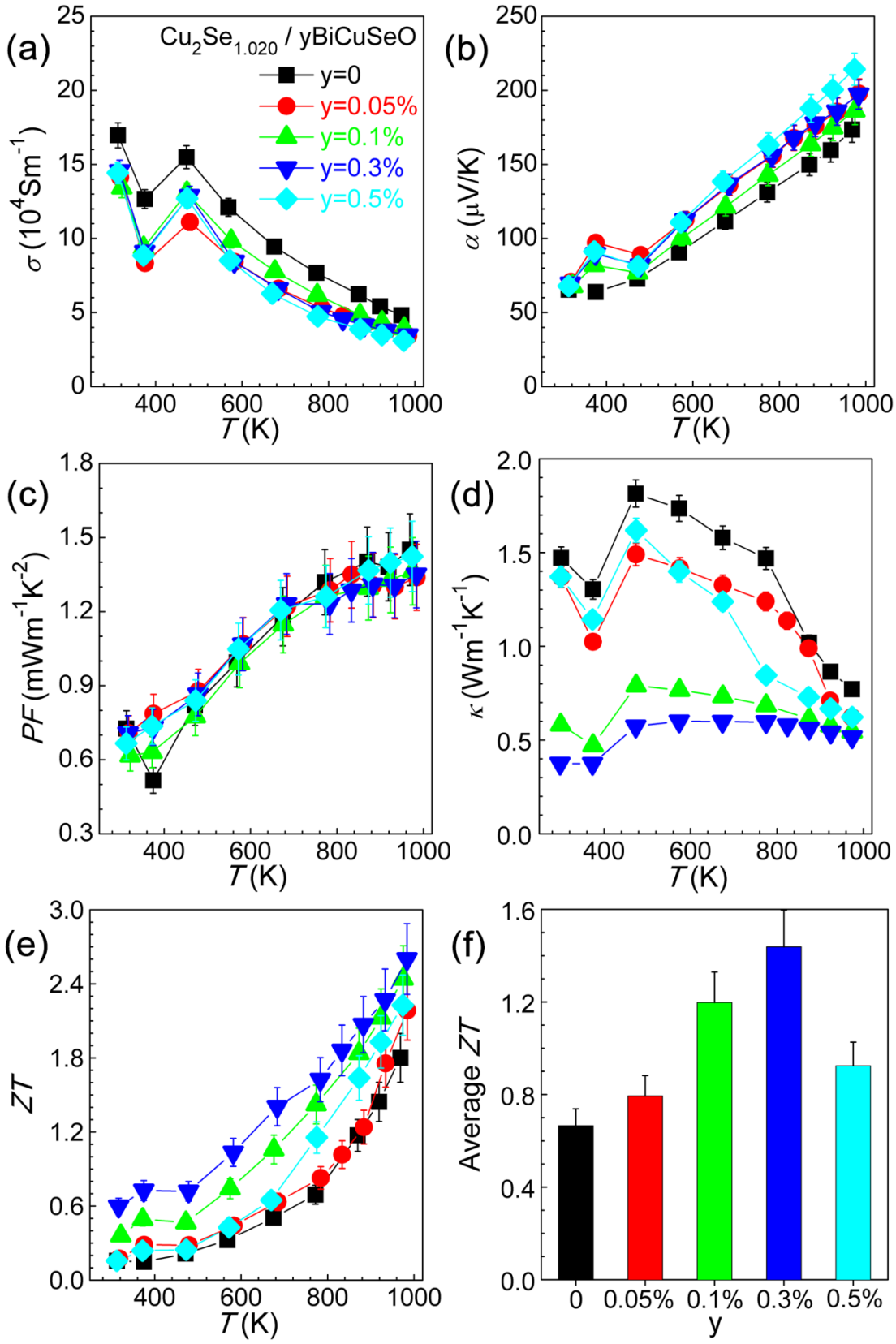

Figure S15. Thermoelectric properties of $Cu_2Se_{1.020}$ / yBiCuSeO. (a) electrical conductivity; (b) Seebeck coefficient; (c) power factor; (d) thermal conductivity; (e) *ZT*; (f) average *ZT* values between 400 K and 973 K.

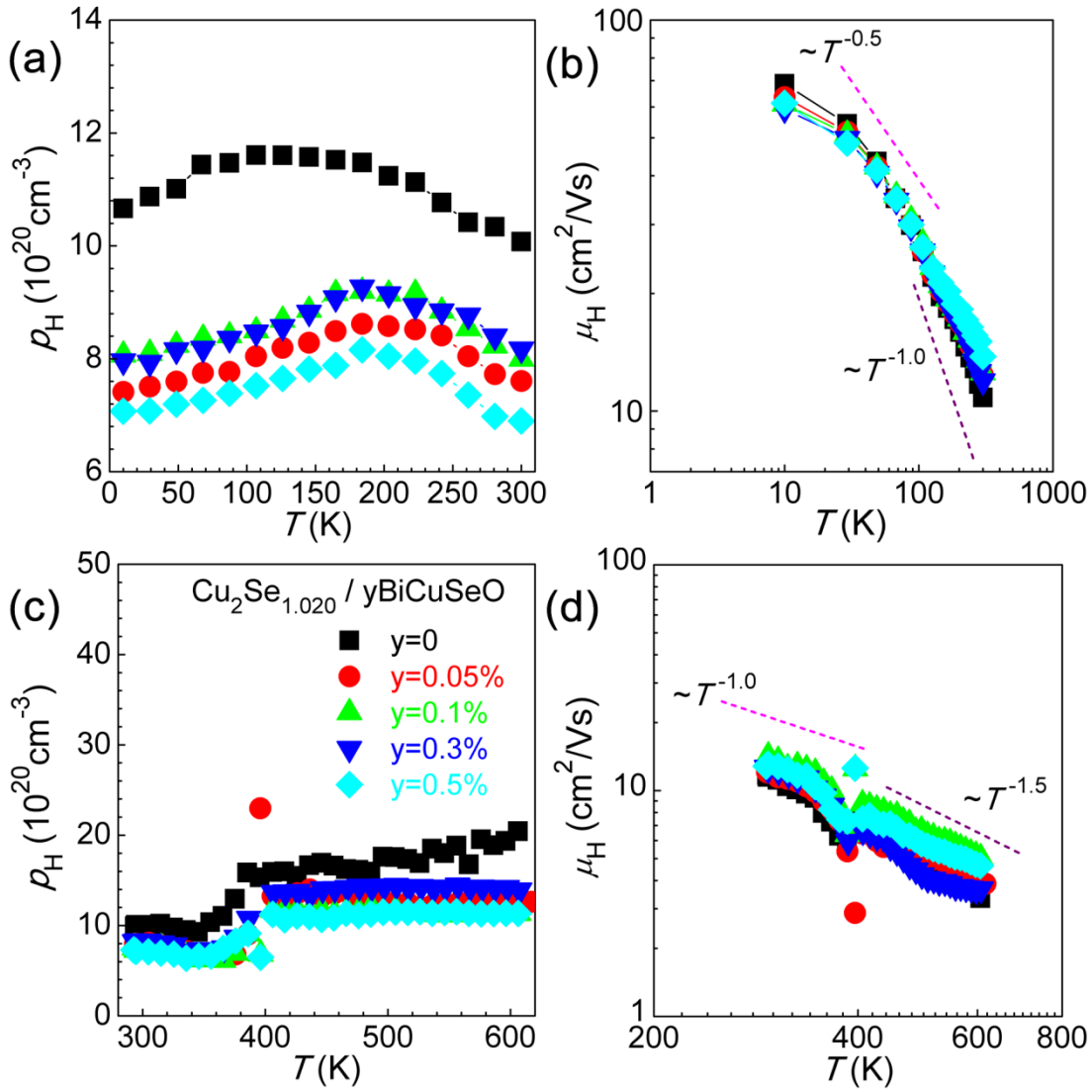

Figure S16. Electrical transport properties of $Cu_2Se_{1.020}$ / yBiCuSeO. (a) low temperature carrier concentration; (b) low temperature carrier mobility; (c) high temperature carrier concentration; (d) high temperature carrier mobility.

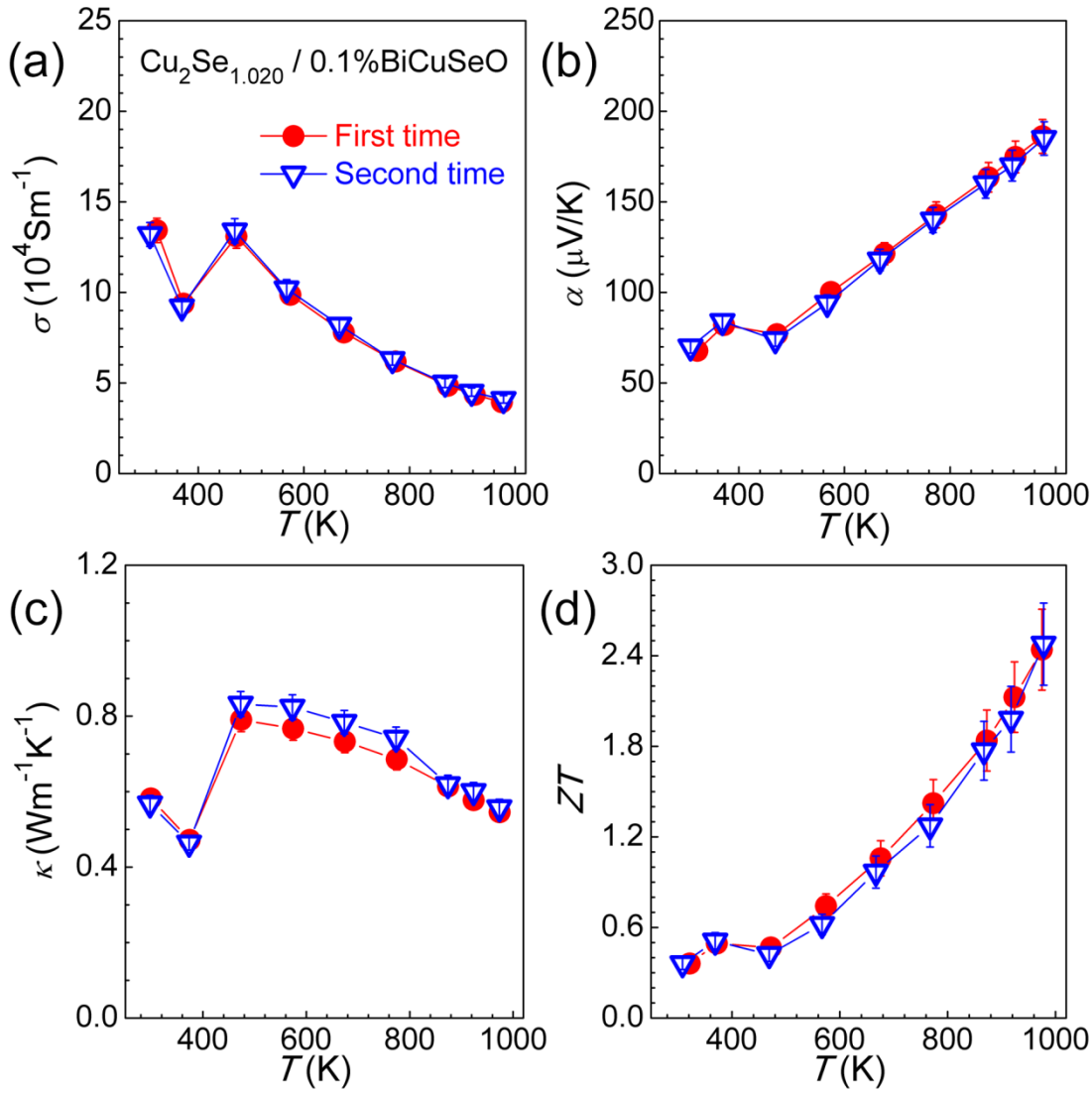

Figure S17. Thermoelectric properties of $Cu_2Se_{1.020}$ / 0.1 mol% BiCuSeO after two thermal cycles between room temperature and 973 K.

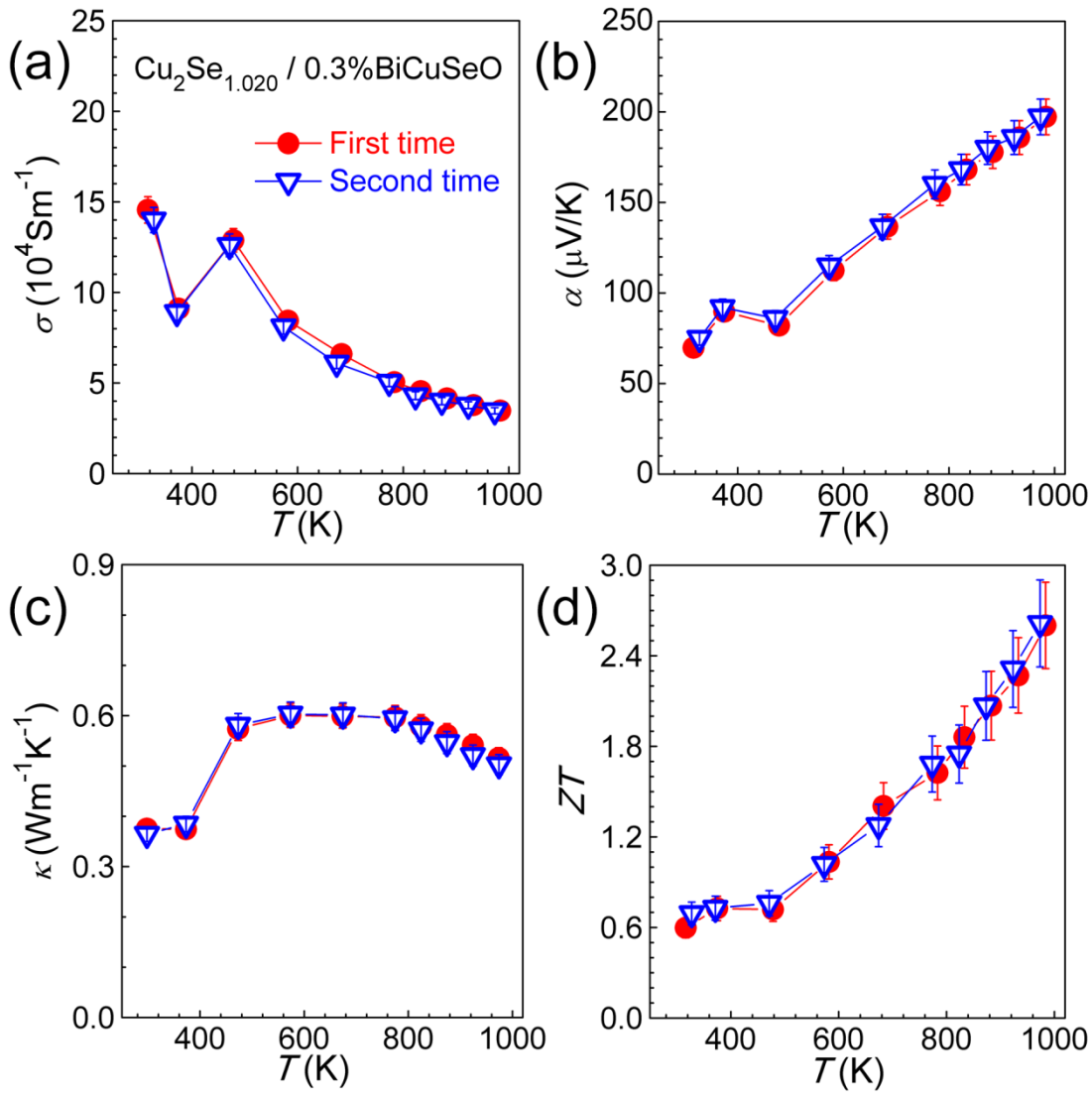

Figure S18. Thermoelectric properties of $Cu_2Se_{1.020}$ / 0.3 mol%BiCuSeO after two thermal cycles between room temperature and 973 K.

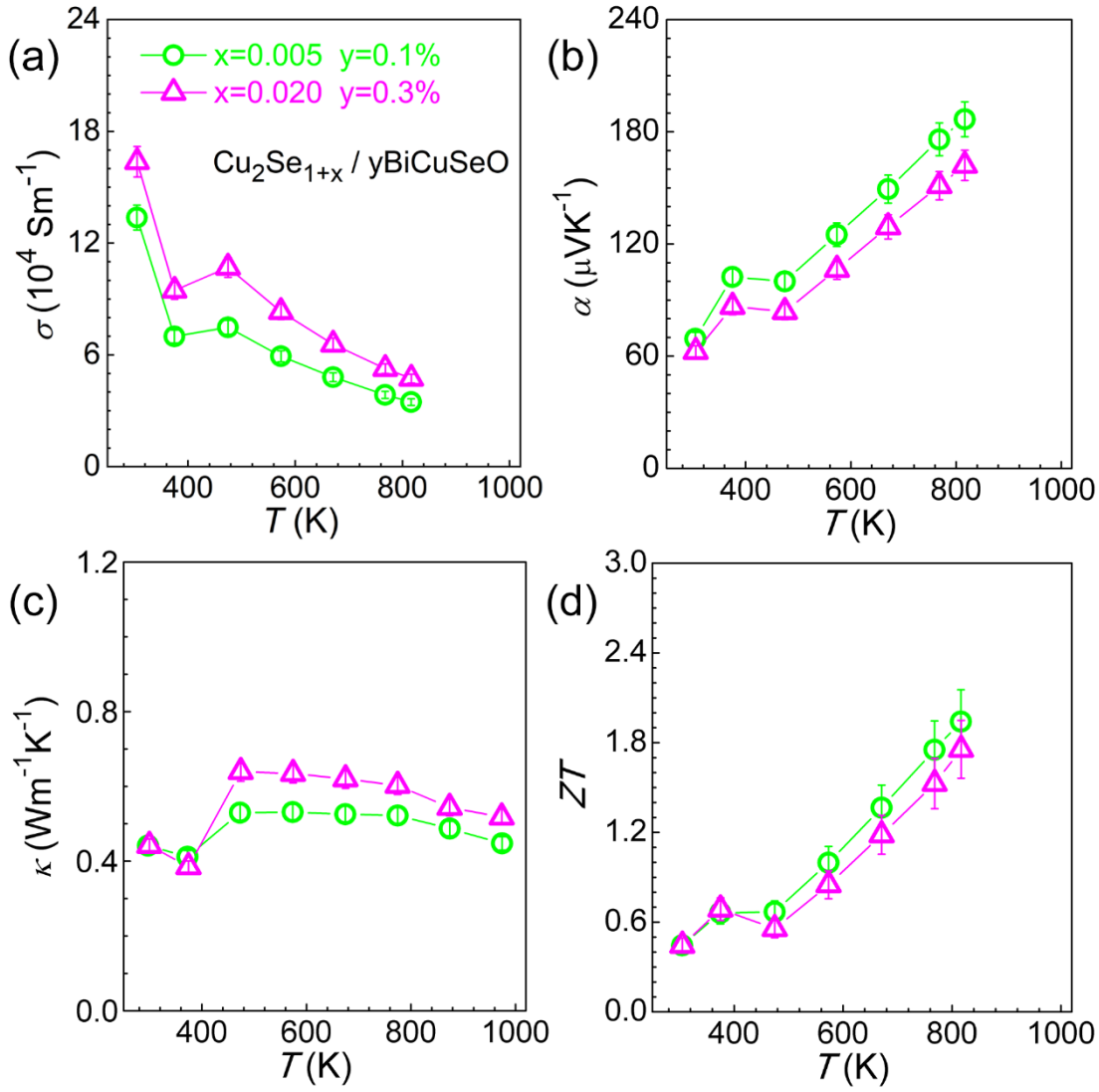

Figure S19. Thermoelectric properties of Cu_2Se_{1+x} / yBiCuSeO composites. Freshly-prepared samples $Cu_2Se_{1.005}$ / 0.1 mol%BiCuSeO and $Cu_2Se_{1.020}$ / 0.3mol% BiCuSeO were cross-checked at the University of Michigan (UM, ZEM-3 in Prof. P. F. P. Poudeu's laboratory) and Huazhong University of Science and Technology (HUST, LFA427 in Prof. Junyou Yang's laboratory). The results agreed well with ours, within the instrumental error.

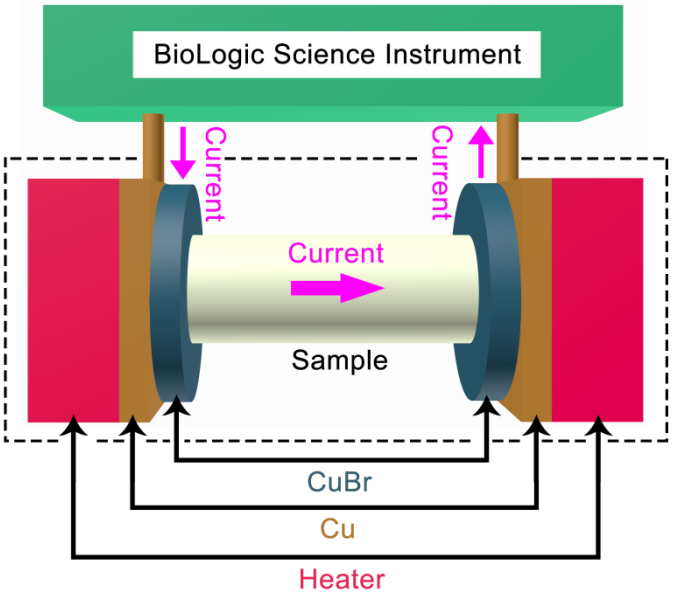

Figure S20. Schematic diagram of a customer designed device for the ionic conductivity measurement. It is based on the electron-blocking method. Two ionic Cu|CuBr electrodes are used to connect with the two ends of the Cu_2Se sample to form a Cu|CuBr|Cu_2Se|CuBr|Cu galvanic cell. These ionic electrodes can block the holes passing across the Cu_2Se|CuBr interfaces while allowing the ions to freely migrate through them. Meanwhile, two ionic Cu|CuBr probes are used to record the potential variation on the sample generated by the movable ions. The total voltage drop is the sum over CuBr and Cu_2Se_{1+x} / yBiCuSeO. When the ionic conductivity of CuBr is known, the ionic conductivity of Cu_2Se_{1+x} / yBiCuSeO can be obtained.

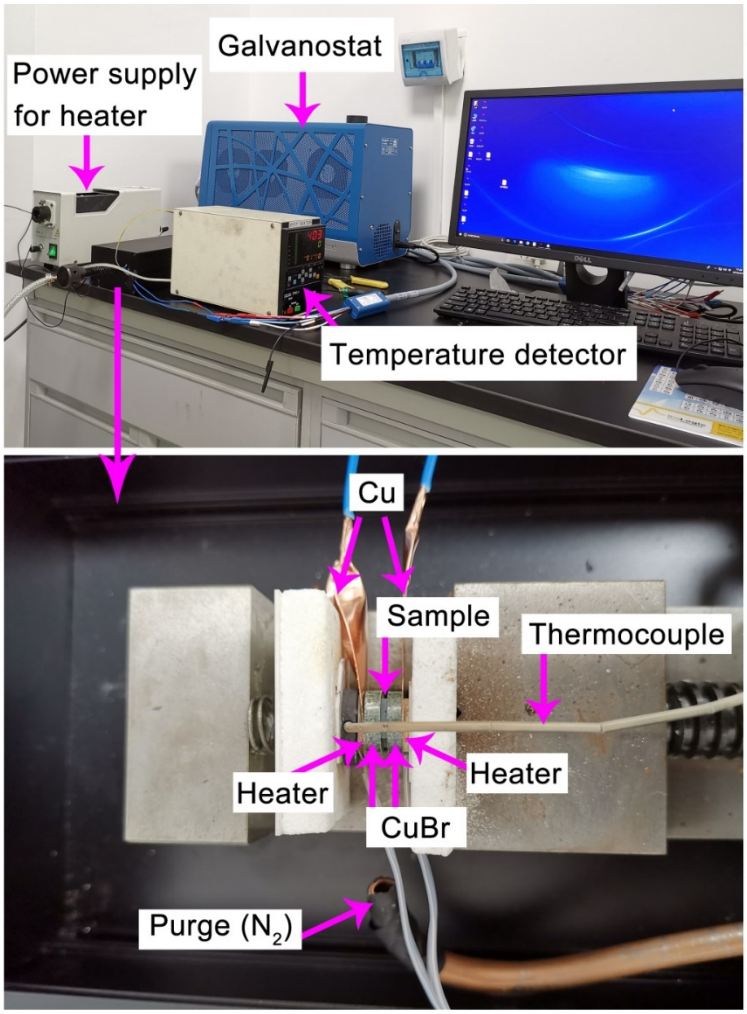

Figure S21. The optical image of the home-made instrument built for the ionic conductivity measurement at about 693 K. The size of CuBr is about $\Phi 12.6 \times 3$ mm^3, while the cross-sectional area of Cu_2Se_{1+x} / yBiCuSeO sample is about 8×8 mm^2.

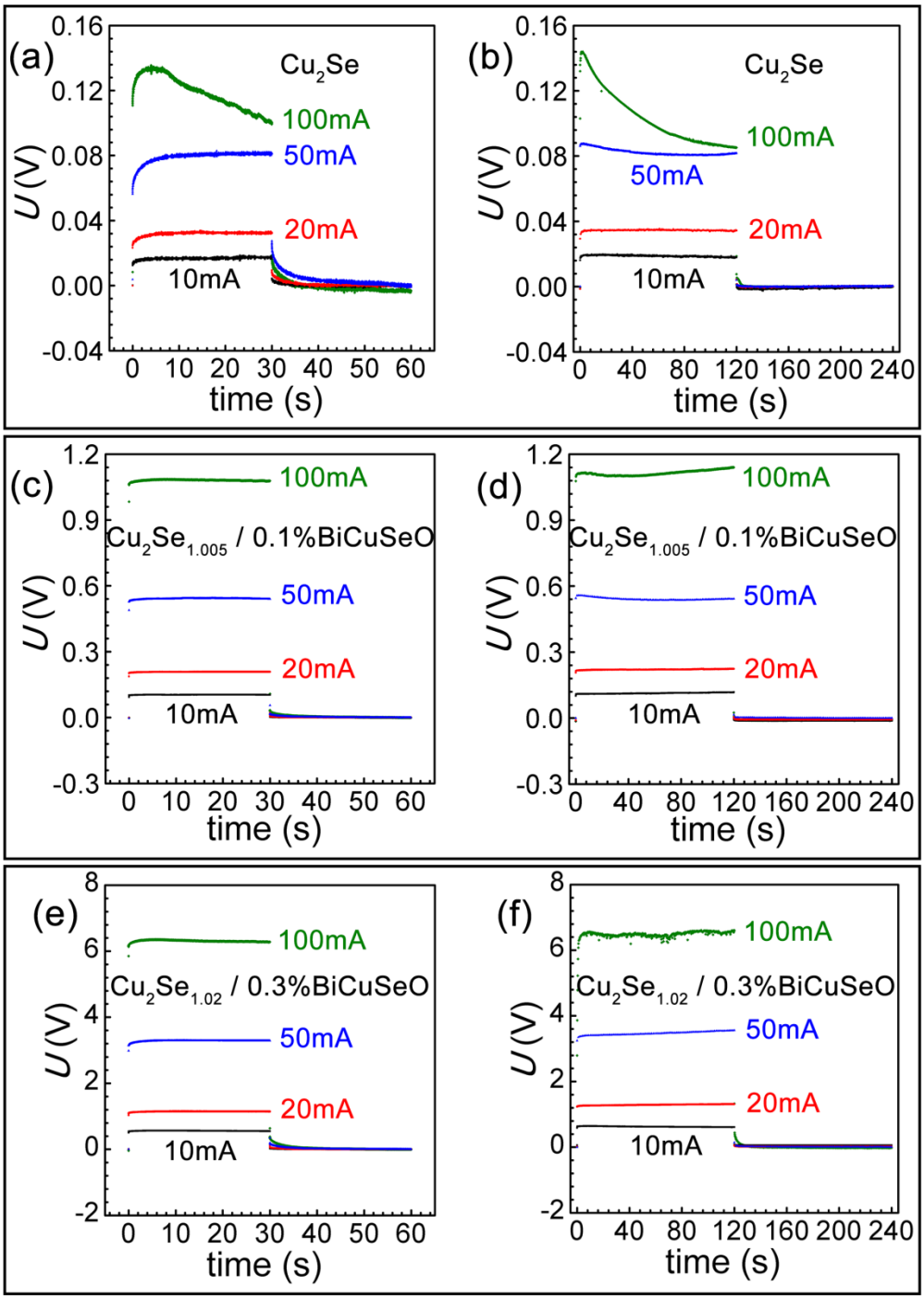

Figure S22. Potential variation curves for Cu_2Se (a-b), $Cu_2Se_{1.005}$ / 0.1 mol% BiCuSeO (c-d), $Cu_2Se_{1.020}$ / 0.3 mol% BiCuSeO (e-f). The test results with 30 s DC polarization and 120 s DC polarization are almost consistent within the range of error.

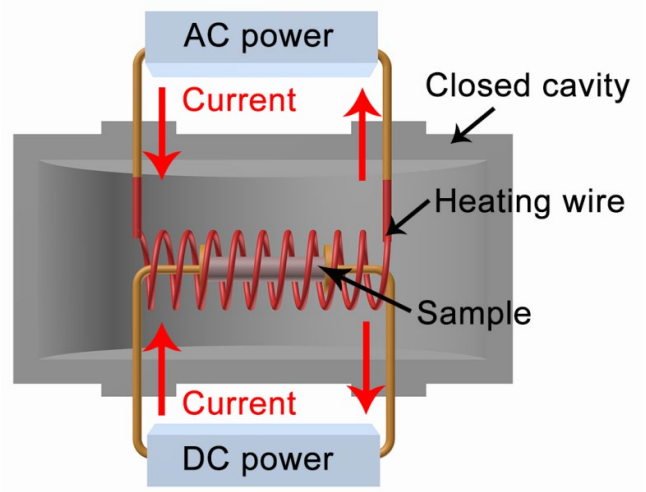

Figure S23. Schematic diagram of a customer designed device for chemical electromigration experiment at constant temperature.

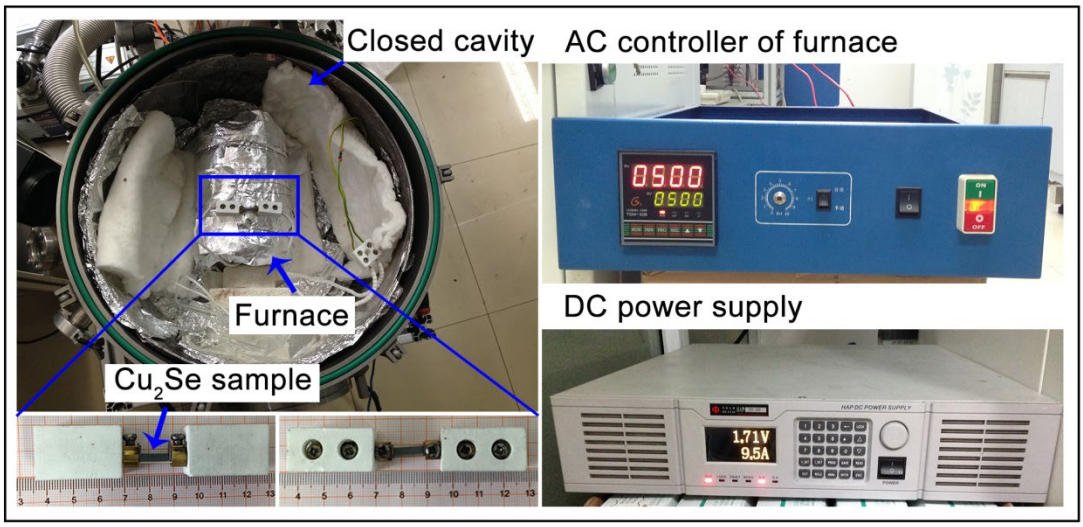

Figure S24. The optical image of the home-made instrument built for the chemical electromigration experiment at constant temperature.

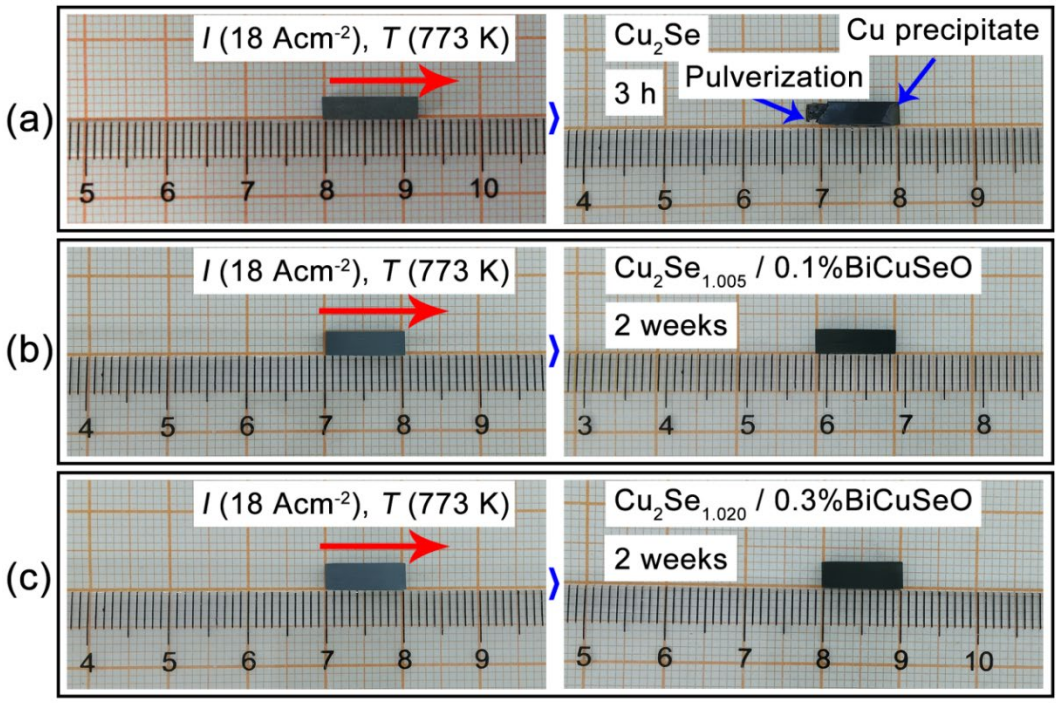

Figure S25. Surface morphology of Cu_2Se_{1+x} / yBiCuSeO composites when the current density of 18 Acm^{-2} was passed through at 773 K.

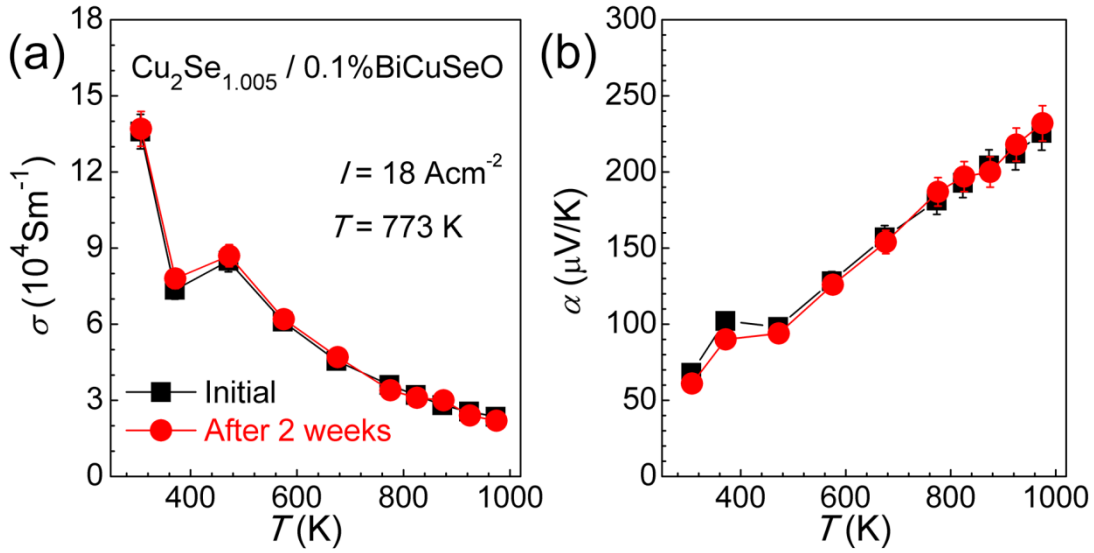

Figure S26. Electrical properties of the $Cu_2Se_{1.005}$ / 0.1 mol%BiCuSeO composite when the current density of 18 Acm^{-2} was passed through at 773 K for 2 weeks. (a) electrical conductivity, (b) Seebeck coefficient.

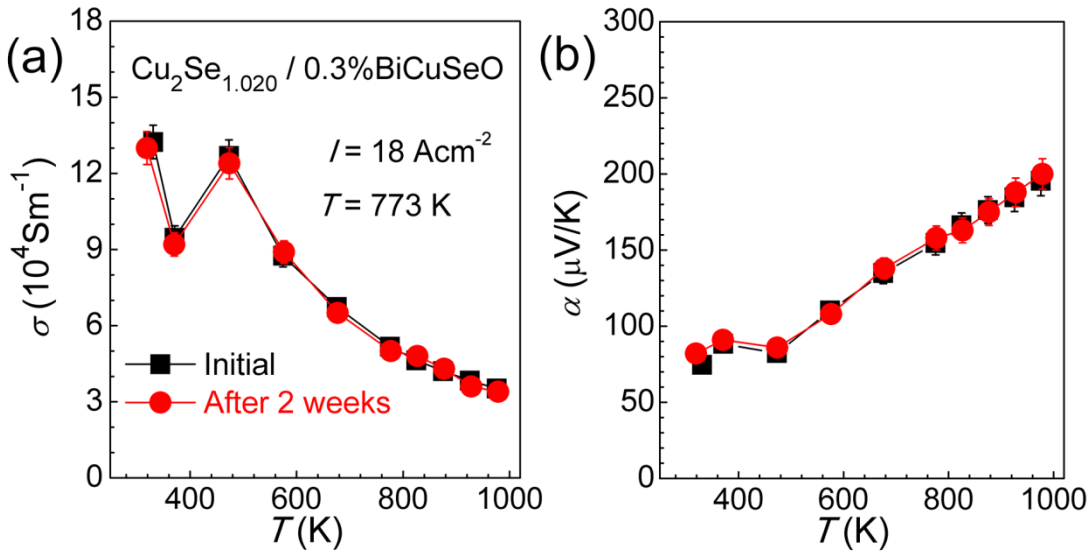

Figure S27. Electrical properties of the $Cu_2Se_{1.020}$ / 0.3 mol% BiCuSeO composite when the current density of 18 Acm^{-2} was passed through at 773 K for 2 weeks. (a) electrical conductivity, (b) Seebeck coefficient.

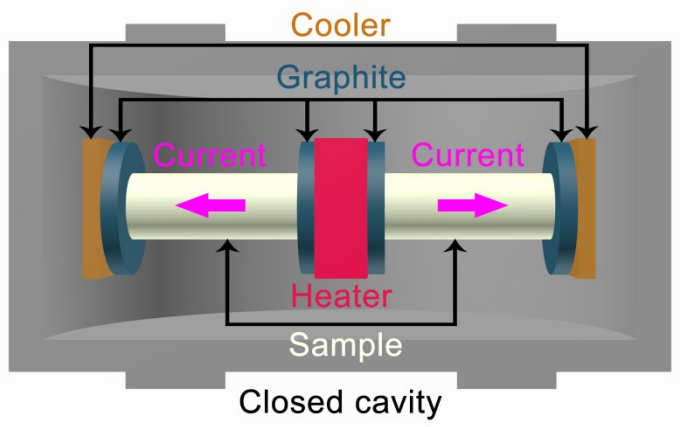

Figure S28. Schematic diagram of a customer designed device for chemical electromigration experiment under a temperature gradient.

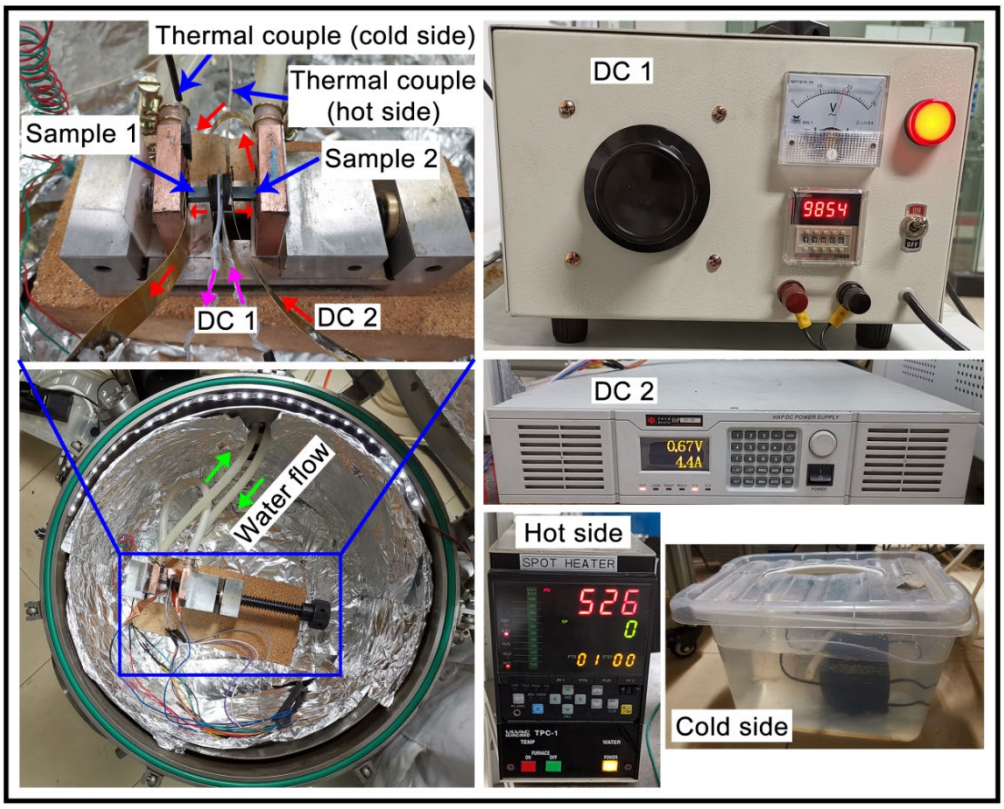

Figure S29. The optical image of the home-made instrument built for the chemical electromigration experiment under a temperature gradient. The low temperature end is cooled to about 293 K with circulating water. The high temperature end is heated to about 793 K with a ceramic heating plate.

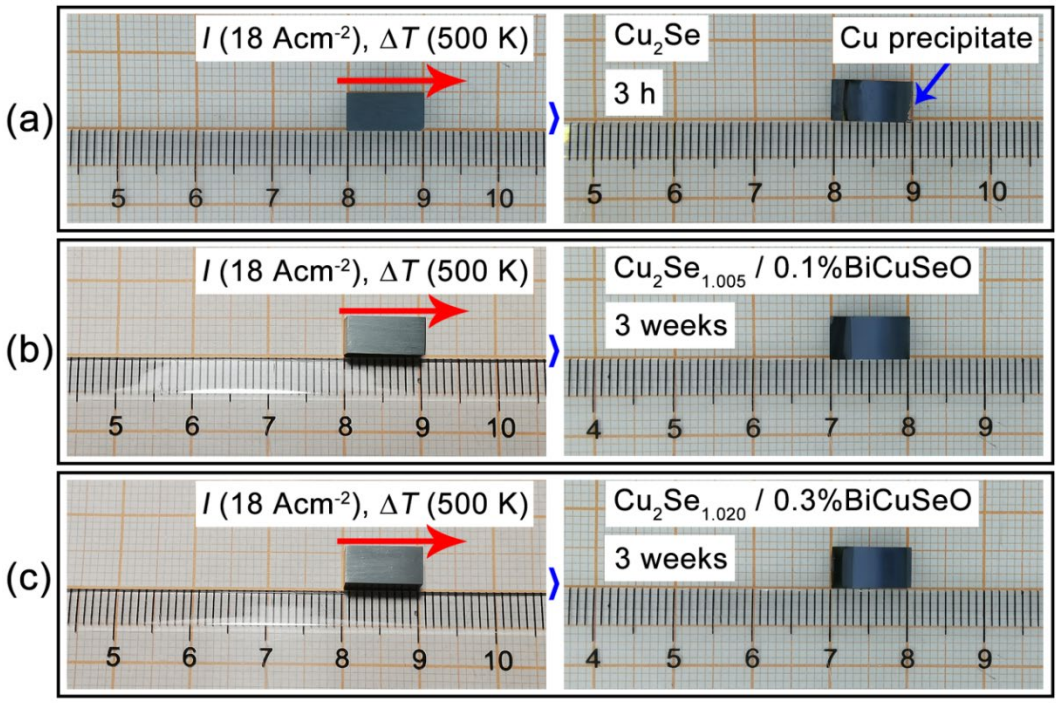

Figure S30. Surface morphology of Cu_2Se_{1+x} / yBiCuSeO composites when the current density of 18 Acm^{-2} was passed through under a 500 K temperature gradient (with the high temperature end at 793 K, and the low temperature end at 293 K).

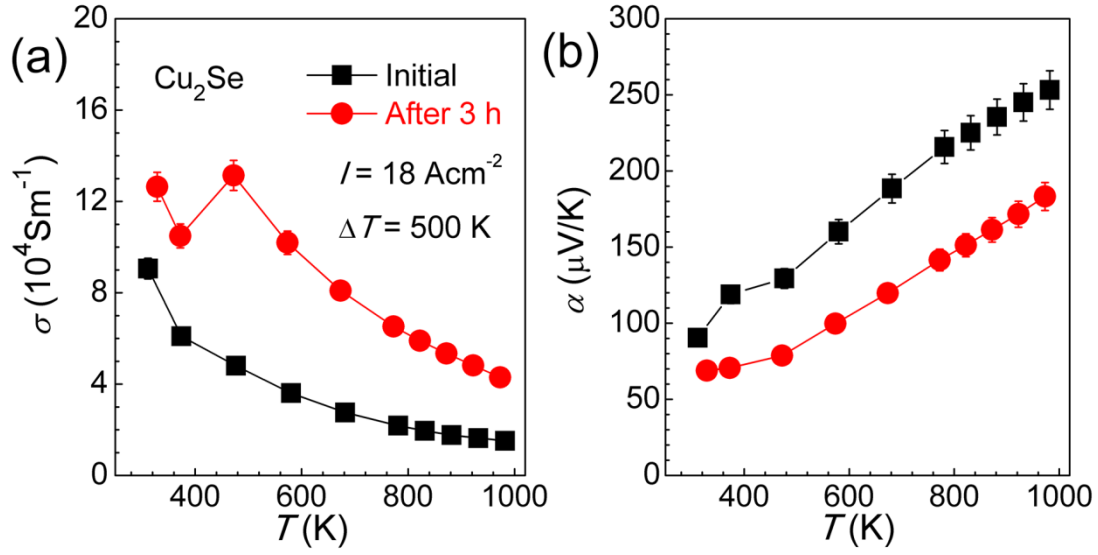

Figure S31. Electrical properties of the Cu_2Se sample when the current density of 18 Acm^{-2} was passed through under a 500 K temperature gradient (with the high temperature end at 793 K, and the low temperature end at 293 K) for 3 h. (a) electrical conductivity, (b) Seebeck coefficient.

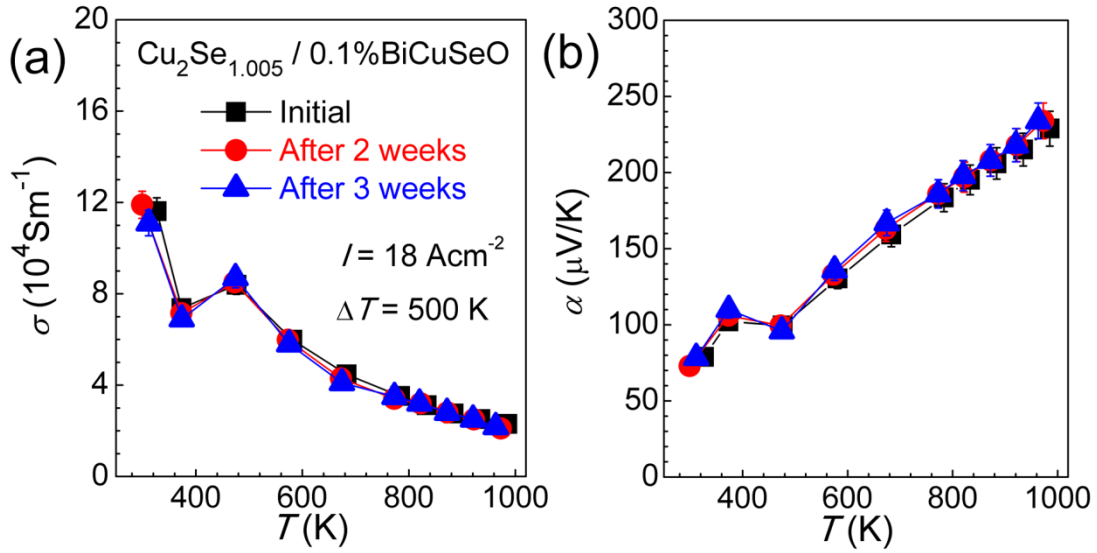

Figure S32. Electrical properties of the $Cu_2Se_{1.005}$ / 0.1 mol%BiCuSeO composite when the current density of 18 Acm^{-2} was passed through under a 500 K temperature gradient (with the high temperature end at 793 K, and the low temperature end at 293 K) for 2 and 3 weeks. (a) electrical conductivity, (b) Seebeck coefficient.

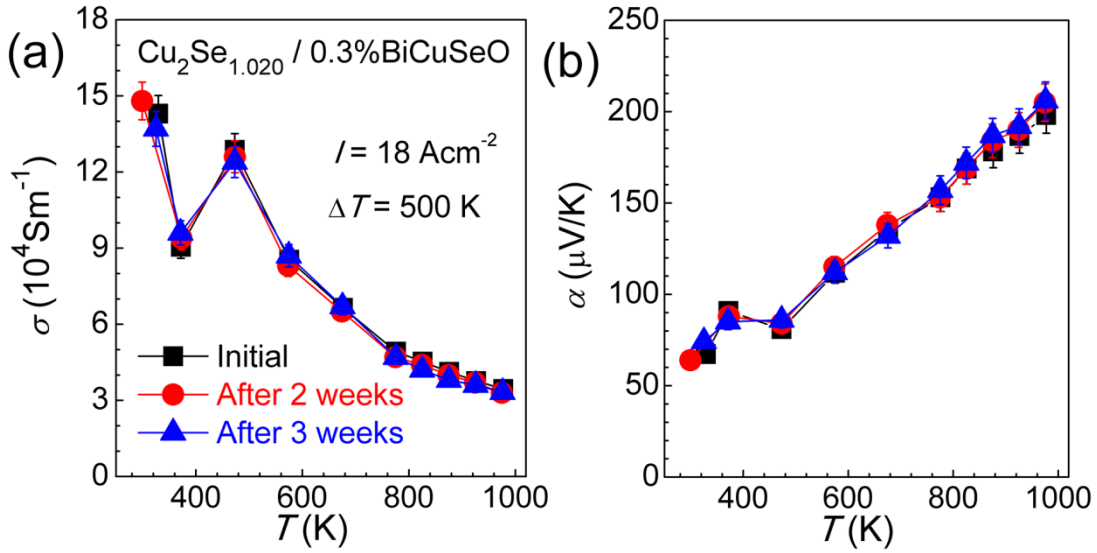

Figure S33. Electrical properties of the $Cu_2Se_{1.020}$ / 0.3 mol%BiCuSeO composite when the current density of 18 Acm^{-2} was passed through under a 500 K temperature gradient (with the high temperature end at 793 K, and the low temperature end at 293 K) for 2 and 3 weeks. (a) electrical conductivity, (b) Seebeck coefficient.

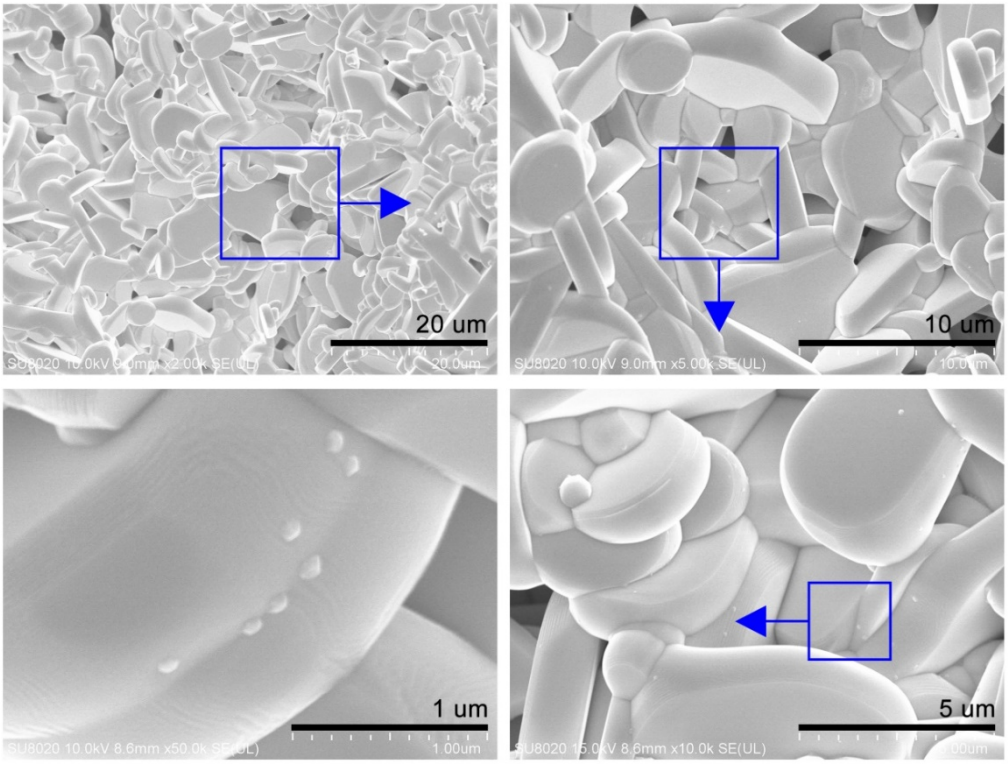

Figure S34 FESEM of Bi_2SeO_2 bulk materials synthesized by thermal explosion technology. Bi_2SeO_2 particle with nm-μm size exhibit nearly polygonal lamellar morphology.

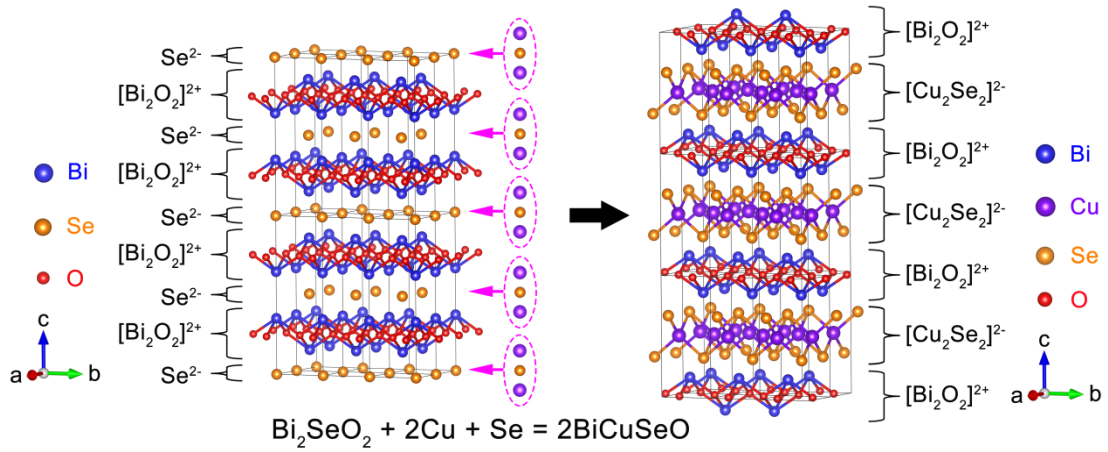

Figure S35 The schematic diagram of crystal structure transformation during the process of Bi_2SeO_2 + 2Cu + Se = 2BiCuSeO.

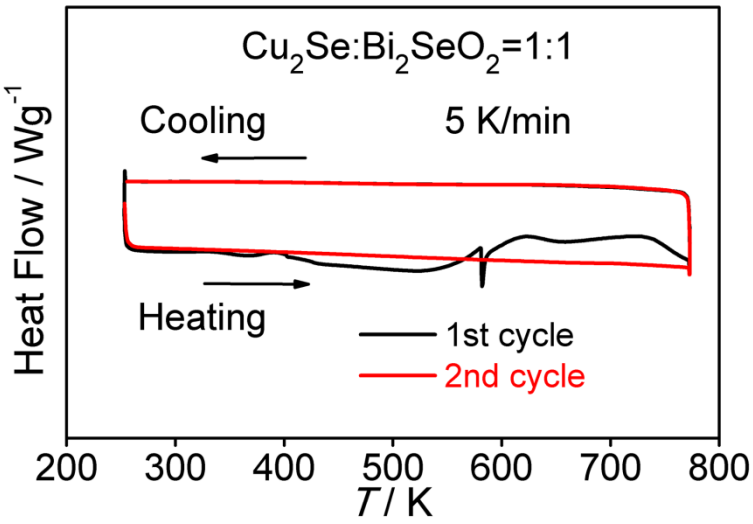

Figure S36. Heat flow of the mixed equimolar powders of Cu_2Se and Bi_2SeO_2. The heating and cooling rates are both 5 K/min. In the first thermal cycle, there is an obvious endothermic peak near 582 K. However, the endothermic peak disappeared in the second cycle, indicating Cu_2Se reacted with Bi_2SeO_2 to form BiCuSeO near 582K.

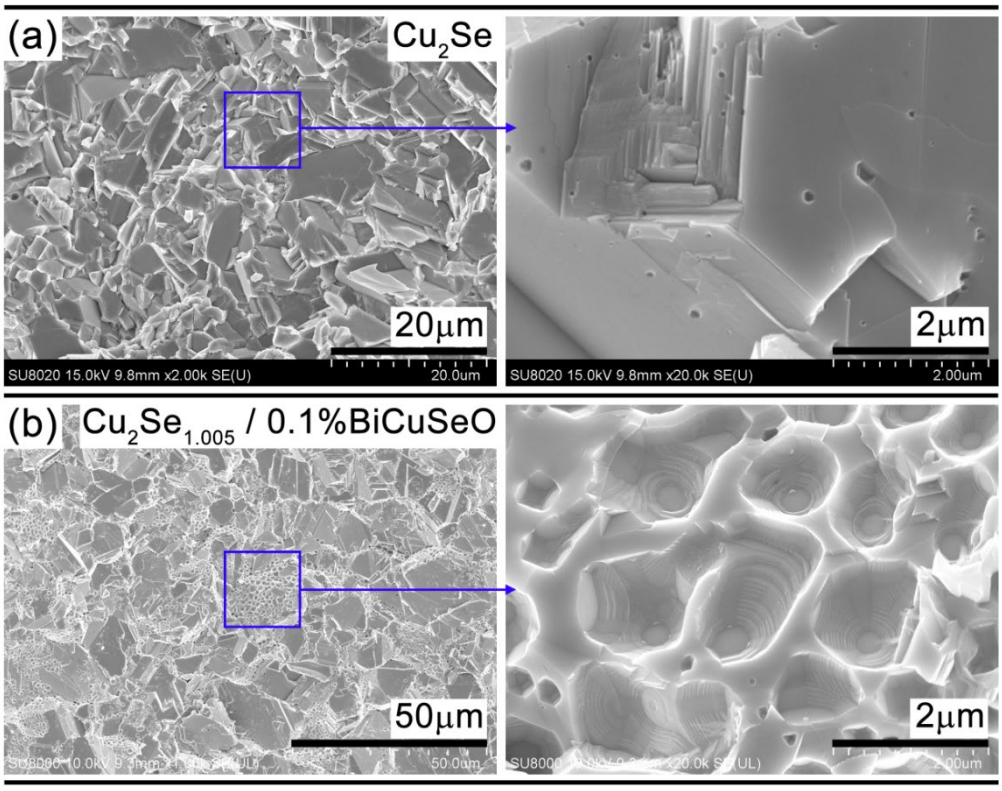

Figure S37. FESEM of bulk materials: (a) Cu_2Se, (b) $Cu_2Se_{1.005}$ / 0.1mol%BiCuSeO. For Cu_2Se, a large number of sub-micron scale closed pits were formed, and the relative density is about 95.4%. For $Cu_2Se_{1.005}$ / 0.1mol%BiCuSeO, due to the introduction of trace BiCuSeO, a larger number of sub-micron scale closed pits were formed, and the inner wall of the pits appeared as a ladder. The relative density is about 94.5%, smaller than Cu_2Se bulk material.

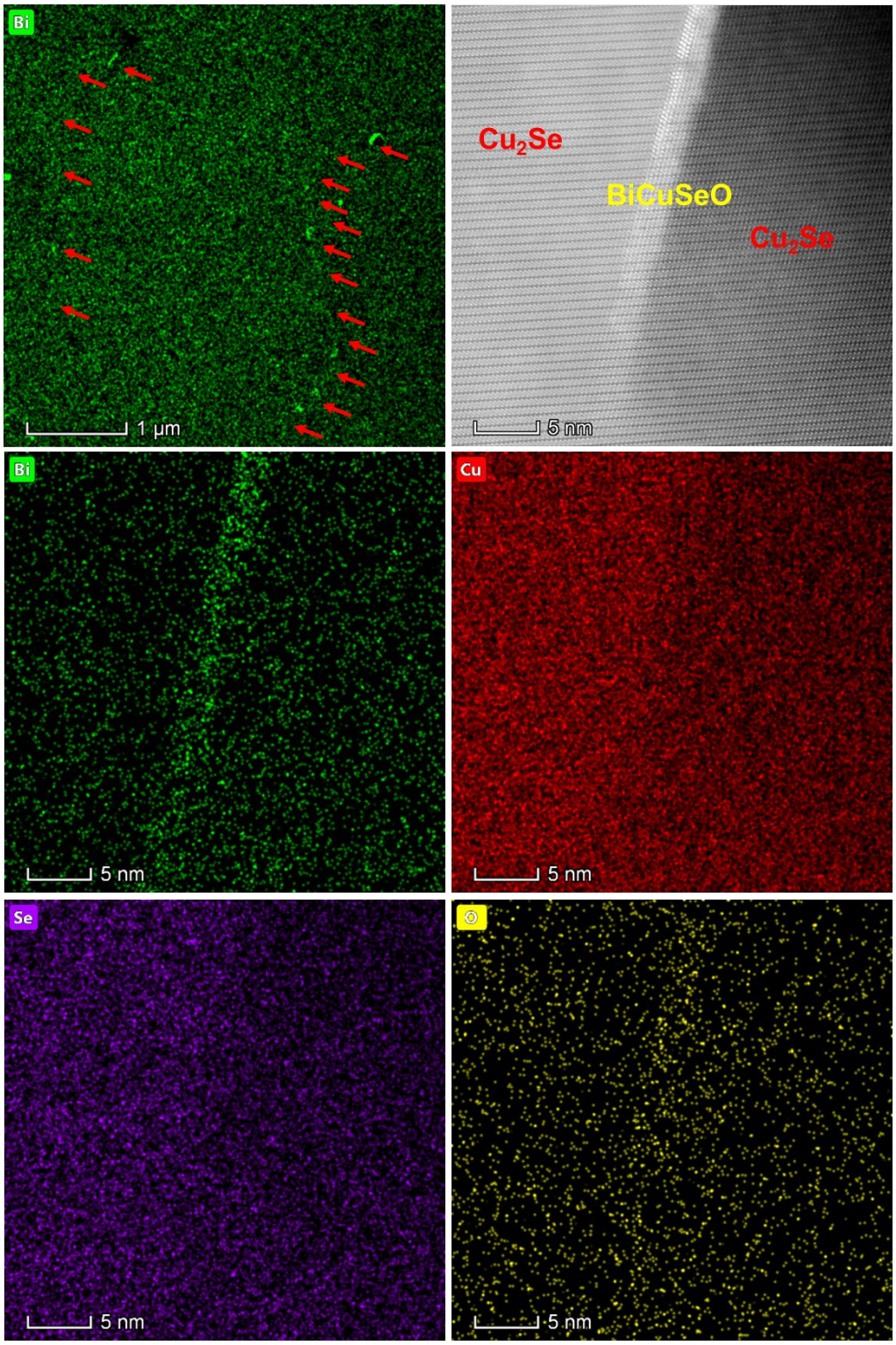

Figure S38. (a) Low magnification EDS elemental map (Bi) of $Cu_2Se_{1.005}$ / 0.1mol%BiCuSeO bulk material in the area without pores; (b) HAADF-STEM image and corresponding EDS elemental maps, Bi (green), Cu (red), Se (purple), and O (yellow). BiCuSeO is distributed in the matrix with a size smaller than 5nm.

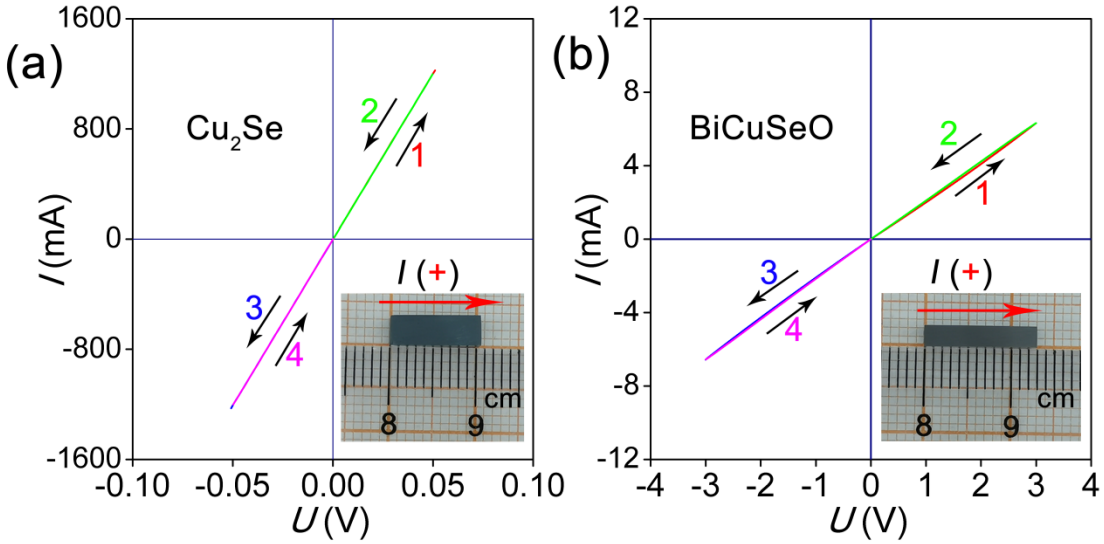

Figure S39. *I-U* curve of Cu_2Se and of BiCuSeO

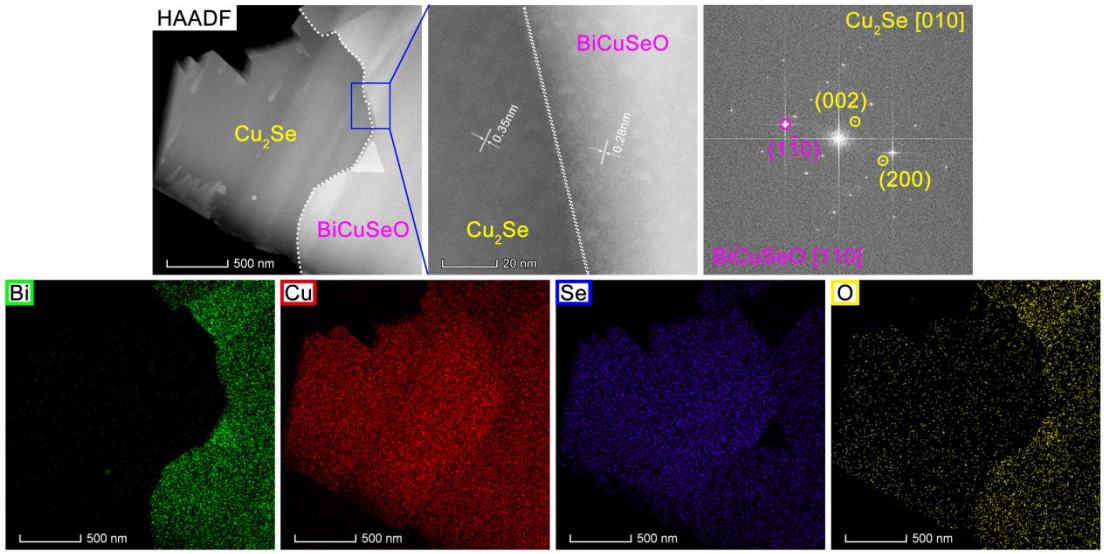

Figure S40. HAADF image, high resolution image and its corresponding diffraction pattern, and EDS mapping results for the Cu_2Se/BiCuSeO heterojunction.

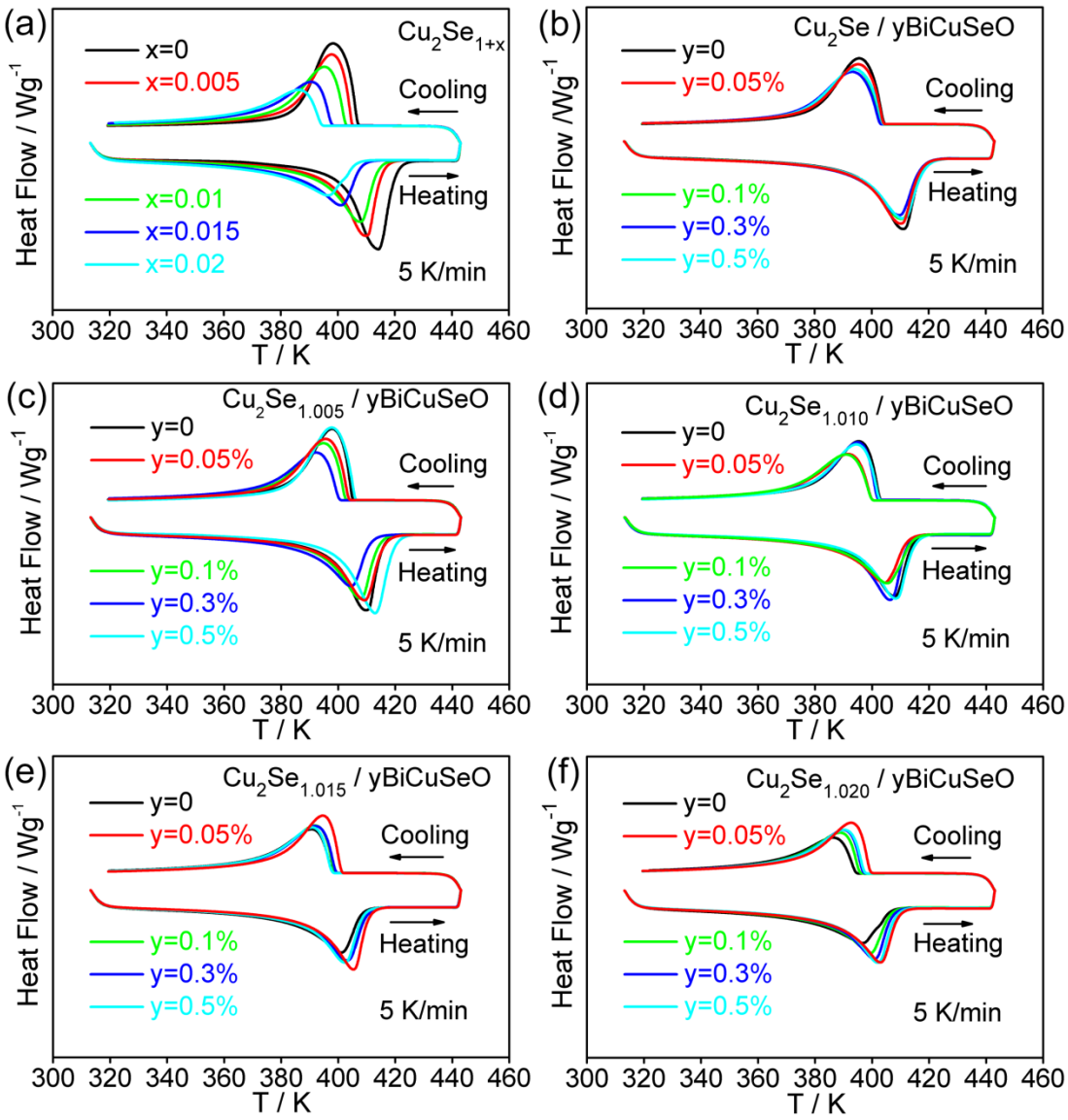

Figure S41. Heat flow diagrams: (a) Cu_2Se_{1+x}, (b) Cu_2Se / yBiCuSeO, (c) $Cu_2Se_{1.005}$ / yBiCuSeO, (d) $Cu_2Se_{1.010}$ / yBiCuSeO, (e) $Cu_2Se_{1.015}$ / yBiCuSeO, (f) $Cu_2Se_{1.020}$ / yBiCuSeO. The heating and cooling rate is both 5 K/min, unless otherwise noted. All the samples have reversible phase transition near 400 K, which corresponds to the α-β phase transition process in Cu_2Se compounds. For Cu_2Se_{1+x} samples, the phase transition temperature (T_{tr}) decreases from 399.2 K to 387.4 K with the increasing Se content. For Cu_2Se / yBiCuSeO, $Cu_2Se_{1.005}$ / yBiCuSeO, and $Cu_2Se_{1.010}$ / yBiCuSeO, after the incorporation of BiCuSeO, the T_{tr} tends to shift to a lower temperature, indicating a decreasing Cu/Se ratio accordingly. For $Cu_2Se_{1.015}$ / yBiCuSeO and $Cu_2Se_{1.020}$ / yBiCuSeO, after the incorporation of BiCuSeO, the T_{tr} tends to shift to a higher temperature, indicating an increasing Cu/Se ratio. The resulting heat flow curve shows that the composite with BiCuSeO can adjust the Cu/Se ratio in the Cu_2Se_{1+x} host matrix in the process of preparation.

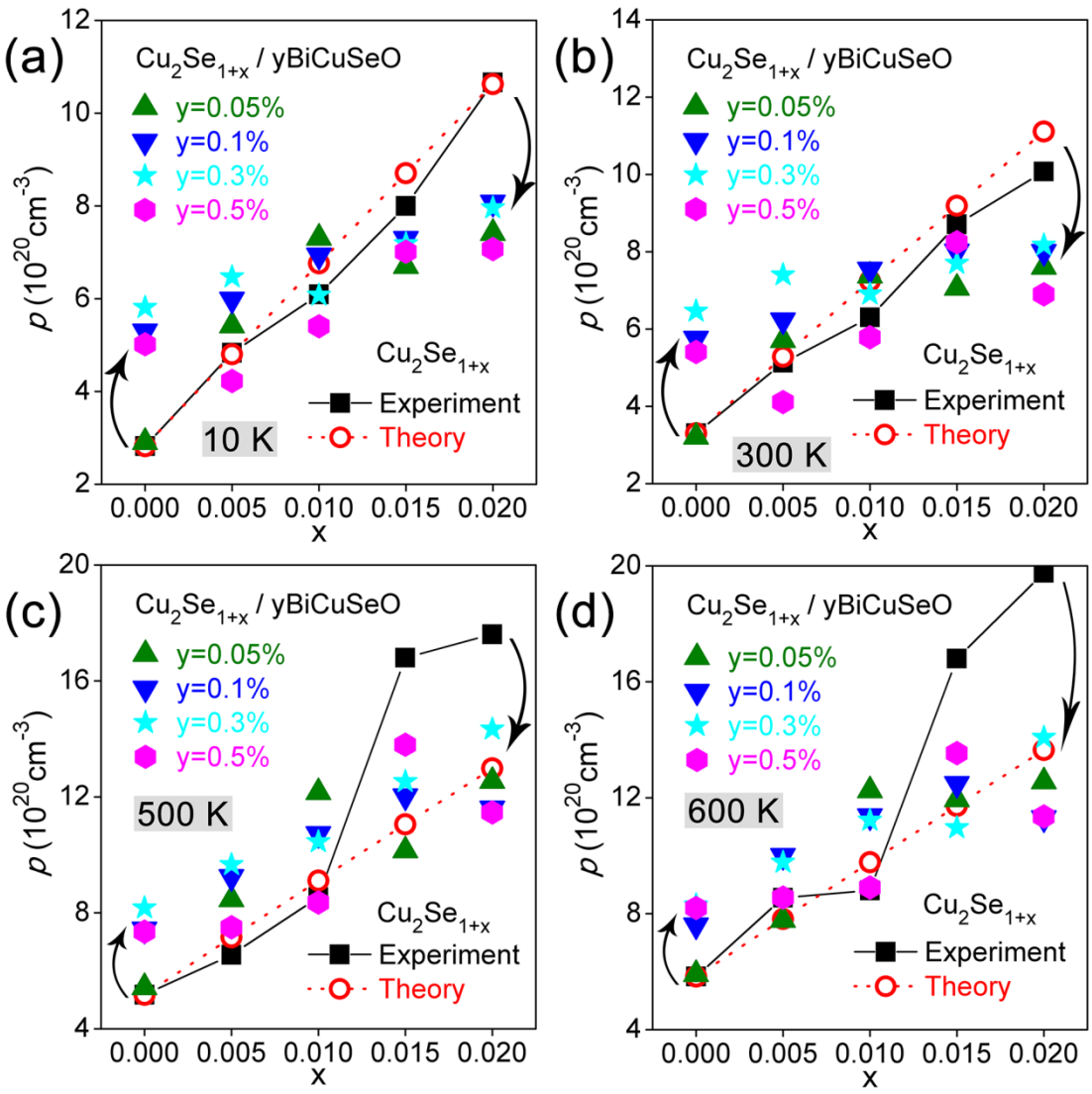

Figure S42. The relation between the carrier concentration and the composition (x, y) at 10 K, 300 K, 500 K and 600 K clearly show the self-regulation of holes upon compositing.

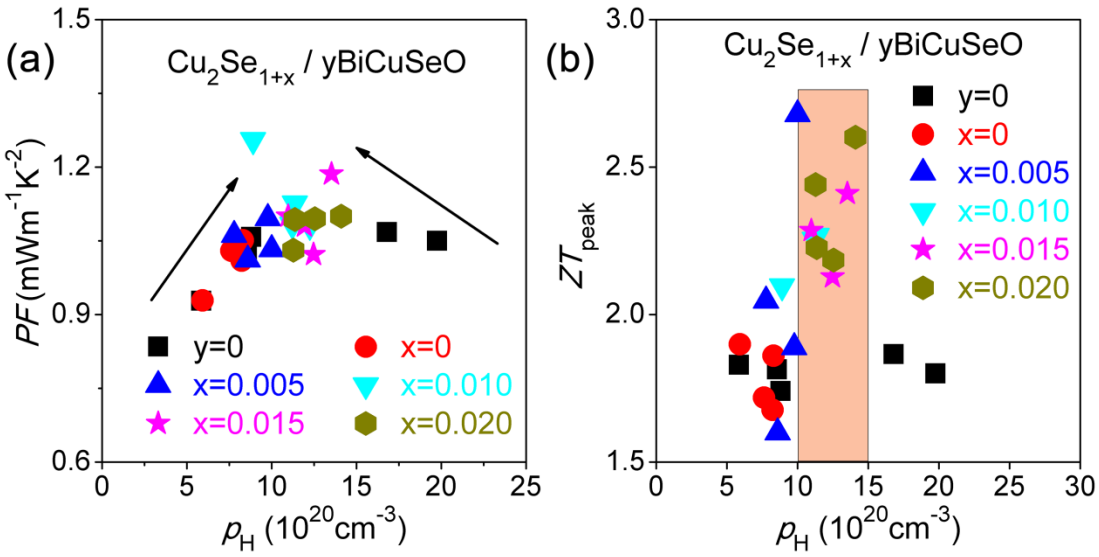

Figure S43. The maximum power factor (a) and peak *ZT* value (b) obtained in the whole temperature range as a function of carrier concentration (at 600K) for Cu_2Se_{1+x}/yBiCuSeO.

Reference:

1. D. W. Yang, X. L. Su, Y. G. Yan, T. Z. Hu, H. Y. Xie, J. He, C. Uher, M. G. Kanatzidis and X. F. Tang, *Chem. Mater.,* 2016, **28**, 4628.
2. V. M. Glazov, A. S. Pashinkin and V. A. Fedorov, *Inorg. Mater.,* 2000, **36**, 641.